ϕ meson properties in dense resonance matter at finite temperature

Manpreet Kaur[*] and Arvind Kumar[†]

Department of Physics, Dr. B R Ambedkar National Institute of Technology Jalandhar, Jalandhar 144008, Punjab, India

(Received 14 May 2025; accepted 26 June 2025; published 16 July 2025)

The effective mass and decay width of the ϕ meson in the isospin asymmetric hot and dense resonance matter are studied using the effective Lagrangian framework considering the $\phi K\bar{K}$ interactions at one-loop level. In addition to spin-1/2 octet baryons, we consider the effect of resonances $\Delta^{++,+,0,-}, \Sigma^{*\pm,0}, \Xi^{*0,-}, \Omega^{-}$, on the properties of ϕ meson. The in-medium effects on the ϕ meson properties are simulated through the effective masses of kaons and antikaons computed using the chiral SU (3) hadronic mean field model in the presence of resonance baryons. The loop integral appearing in the computation of ϕ meson self-energies is regularized using the dipole form factor with a cutoff parameter. The presence of resonance baryons within the medium at finite temperature is observed to significantly modify the effective mass and decay width of ϕ mesons. Examining the ϕ meson masses and decay width within a dense medium is anticipated to be essential for understanding experimental results from heavy-ion collision experiments.

DOI: 10.1103/h2ll-5js4

I. INTRODUCTION

The in-medium hadron modifications have been identified as a crucial component for interpreting the nonpertubative domain of QCD, which predicts several phases of matter at finite density and temperature [1,2]. As a result, essential investigations in this sector are both attractive and challenging. Because of the property of QCD confinement, at low temperature and moderate density, hadrons are treated as the degree of freedom in dense matter. However, at high temperature and density, these hadrons are anticipated to liberate quarks and gluons, forming the quark-gluon plasma [3,4]. Gaining insight into the hadron-quark phase transition, where chiral symmetry is believed to be restored, requires examining the fundamental properties of hadrons and quarks as well as their interactions at finite densities. Understanding the thermodynamic properties of QCD plays a vital role in resolving natural events like compact stars and experimental findings from relativistic heavy-ion collisions (HICs) [1,2,5–8]. The heavy-ion collision experiments performed at very high center-of-mass energy such as Au-Au collisions at the relativistic heavy ion collider (RHIC), with $\sqrt{S_{NN}} = 200$ GeV [9–12] and Pb-Pb collisions at the LHC [13,14], with $\sqrt{S_{NN}} = 2.76$ TeV, explore the QCD phase transition at high temperatures and low baryonic densities. Further insights are expected from forthcoming experiments, including the Compressed Baryonic Matter (CBM) [15,16], Antiproton Annihilation at Darmstadt (PANDA) [17,18], of the Facility for Antiproton and Ion Research (FAIR) at GSI [19], Japan Proton Accelerator Research Complex (J-PARC Japan) [20,21] and Nuclotron-based Ion Collider Facility (NICA) at Dubna, Russia [22,23], focusing on the physics of dense matter at finite baryonic densities.

The hadrons produced in different HICs have a short lifetime, and they decay with considerable probability within the strongly interacting environment. In HICs, there are a number of reasons to be interested in measuring the in-medium modifications of light vector mesons, such as the large-scale production of these mesons account for roughly 15% of the total particle yields, their short lifetime, and significant electromagnetic decay properties. These properties make them valuable for examining the dense and hot hadronic matter through the dilepton pairs, which provide spectral knowledge of the vector mesons at the time of decay [1,24].

QCD becomes highly challenging to solve in the nonperturbative low-energy regime because of the strong coupling of gluons and quarks. Consequently, researchers have explored alternative approaches to characterize hadrons within dense matter. The primary theoretical tools to explore the in-medium properties in the nonperturbative domain of QCD are (i) lattice QCD calculations and

[*]Contact author: ranapreeti803@gmail.com
[†]Contact author: kumara@nitj.ac.in

Published by the American Physical Society under the terms of the Creative Commons Attribution 4.0 International license. Further distribution of this work must maintain attribution to the author(s) and the published article's title, journal citation, and DOI. Funded by SCOAP[3].

(ii) phenomenological models. To investigate the QCD phase diagram in the sector of the high temperature and low baryonic density, one can use the lattice QCD simulation method, which is based on space-time grid points [25]. However, when the density of baryons rises, the sign problem with the fermion determinant causes lattice QCD to be inefficient, which leads to higher computational costs and lower productivity [26–30]. Various phenomenological models and approaches have been developed to investigate hadronic matter outside the lattice QCD framework. These include quark meson coupling model [31–33], the Nambu–Jona-Lasinio (NJL) model [34], the linear-sigma model [35], the hadron resonance gas model [36], the Dyson-Schwinger equation approach [37], chiral perturbation theory [38–40], QCD sum rules [2,41,42], the chiral SU(3) hadronic and quark mean field model [43–52], the Polyakov quark meson model [53–55], the Polyakov loop extended NJL (PNJL) model, and the coupled channel approach [56–64]. Theoretical studies have broadened their reach by covering a variety of factors, including the exploration of nonextensive properties [65,66], the impact of the external magnetic field [67–69], the implications of finite system sizes [70–72], and the examination of how electric fields influence the thermodynamics of strongly interacting systems [73,74].

In HICs, even at relatively low energies, several kinds of mesons; nonstrange and strange baryons; and pions, nucleons, and resonances are produced. The production of strangeness in these collisions and neutron stars is of considerable interest because they provide a way to answer many fundamental questions of nuclear and hadronic physics connected to the many concepts of QCD [5,75,76]. Because of the conservation of strangeness in hadronic reactions, the production of strange hadrons is essential. The production of open strangeness occurs through the creation of kaon-hyperon combinations or the formation of kaon and antikaon pairs $K\bar{K}$. It is possible to produce the hidden strangeness through the ϕ $(s\bar{s})$ meson. There are two ways to measure the ϕ meson. The first involves analyzing the dilepton decay ($\phi \to e^+e^-$ or $\phi \to \mu^+\mu^-$), which offers undistorted information about ϕ meson's behavior within the medium because of negligible interaction of the dileptons with baryons and mesons. However, this approach is challenging because of the low branching ratio of ϕ meson to dileptons. The second method examines $K\bar{K}$ pairs resulting from ϕ meson decay with a high branching ratio [77]. The ϕ meson dominantly decays into the kaon-antikaon pair due to the suppression of ϕ decay via the π meson, a consequence of the Okubo-Zweig-Iizuka rule [78–80].

Numerous theoretical [41,81–89] and experimental [1,2,90–93] investigations have been conducted to examine the properties of the ϕ meson within strongly interacting hadronic matter. In HICs, the ϕ meson has been experimentally observed in both e^+e^- and K^+K^- invariant mass spectra, ranging from energies 1–2 GeV at GSI Helmholtz Centre for Heavy Ion Research to 2–5 TeV at LHC [94]. However, the mass shift of ϕ meson was found to be relatively negligible compared to their lifetime; i.e., a large considerable broadening in decay width of ϕ has been noted. Such broadening results because of the change in the hadronic decay channels and collision processes due to hadron-hadron scattering interactions [1,2]. The E325 experiment at KEK [90] was an earlier experiment that investigated the in-medium modification of ϕ meson by measuring its decay into e^+e^- and $K\bar{K}$ pairs in $p+A$ collisions, observing no modification of invariant mass spectra of $K\bar{K}$ at nuclear saturation density. In Ref. [93], the SPring8 Collaboration, which employed a Glauber-type multiple scattering theory and the A-dependence of ϕ photoproduction yields, observed a significant ϕN cross section in the medium, leading to a decay width of 35 MeV, which aligns with the experimental findings. Further, to improve the statistics significantly, the J-PARC E16 and E88 experiments [94,95] have been proposed as the successors to the E325 experiment, to explore the origin of QCD mass by examining the spectral change of ϕ meson within the nuclear medium [94].

From a theoretical point of view, various approaches such as QCD sum rules [41,81,82], the Nambu–Jona-Lasinio model [83], effective Lagrangian approaches [84–87] have been established, which claim a decrease of ϕ meson mass in the dense nuclear medium. In addition to this, the coupled-channel approach examines kaon-hyperon interaction, incorporating multiple channels and resonances [56,96,97]. These results are further used to determine the modification of in-medium properties of ϕ meson [98]. In Ref. [99], Gubler and Ohtani report the in-medium results of ϕ meson using the QCD sum rule approach. Their findings revealed that the mass shift of ϕ within nuclear matter is closely linked to the nucleon strangeness content σ_{SN} and, based on the value of σ_{SN}, the ϕ meson may experience either an increase or decrease in the mass at nuclear saturation density. Various relativistic transport models have also been employed to examine ϕ meson production in HICs [77,100,101]. For instance, the Parton-Hadron-String Dynamics (PHSD) transport model focuses on interactions between the baryon and baryon and the meson and baryon. The PHSD calculations, which incorporate medium-modified effects like the collisional broadening of the spectral function of the ϕ meson, successfully replicated the experimentally observed K/ϕ ratio [77]. As discussed in Refs. [100,101], the reduction in ϕ meson yield is primarily due to a rise in its decay width resulting from the reduction in kaon-antikaon masses. The study of in-medium masses of ϕ mesons is also important to explore the possible formation of their bound states with different nuclei [89,102–104]. Moreover, recent studies in Refs. [105,106] have examined how the ϕ meson affects neutron stars and hyperon stars within the framework of the relativistic mean field model.

In this work, we employ the chiral SU(3) hadronic model to investigate the in-medium ϕ meson mass and decay width in isospin asymmetric resonance matter. Several studies have addressed resonance production in different collision systems measured by ALICE at LHC [8,107–110]. These studies give information about the final state of hadronic reactions. The chiral perturbation theory [111], NJL and PNJL model [112], and thermal QCD sum rules [113,114] have been used to examine temperature effects on the masses of decuplet baryon Δ, Σ^*, Ξ^*, and Ω^-. QCD sum rules were employed to analyze the in-medium masses of heavy decuplet baryons in symmetric nuclear matter [115]. In Ref. [116], self-energy of Δ, Σ^*, Ξ^*, and Ω^- decuplet baryons within nuclear matter at zero temperature has been studied using the chiral perturbation theory. The chiral SU(3) quark mean field model was utilized to study in-medium masses and magnetic moments of decuplet baryons in nuclear and hyperonic medium [117–120]. Dense resonance matter properties at zero temperature were investigated using the chiral SU(3) model [121]. Heavy baryon resonance properties in nuclear matter have also been studied [119,122]. The influence of resonance baryons, particularly Δ resonances, on compact star mass-radius relations has been explored using various approaches [123–126]. The study of resonance matter properties will also be of significance from the point of view of the PANDA experiment at FAIR and NICA facility where multistrange baryons might be produced. The study of resonance baryons at high temperature (near 150 MeV) might also be of significance in the context of HICs at the RHIC and LHC where such states might be produced during the initial stages of the hadronic phase [8,127].

Keeping in view the above theoretical studies for the properties of resonance matter and future planned experimental facilities for exploring the properties of dense matter, it is important to investigate the in-medium properties of mesons under different environments. Although the properties of ϕ mesons have been investigated extensively in nuclear matter, work needs to be done to investigate how the properties of these mesons might be modified in a medium comprising of resonance baryons in addition to nucleons and hyperons. In the ϕ meson decay, we examine the $K\bar{K}$ loop contributions by solving the effective Lagrangian of the $\phi K\bar{K}$ interaction. Furthermore, with the help of regularization techniques, we evaluate loop integral for in-medium self-energy. This paper is organized in the following manner. Sections II A and II B address the chiral SU(3) hadronic mean field model [45] used to obtain the in-medium scalar and vector fields in dense resonance matter and subsequently the in-medium masses of kaons and antikaons. The theoretical perspective to estimate the in-medium modifications of ϕ meson is explored in Sec. II C. Section III provides the results and discussions, and we conclude with the summary in Sec. IV.

II. METHODOLOGY

The chiral SU(3) hadronic model is applied in the current study to probe the influence of isospin asymmetry and strangeness fraction on the thermodynamic properties of hadronic matter by mesonic exchange (σ, ζ, δ, ω, ρ, and ϕ). Furthermore, we use a self-consistent Lagrangian technique to compute the in-medium properties of the ϕ meson. In the following subsections, we concisely explain the basic formalism used to derive the results for ϕ meson properties.

A. Chiral $SU(3)_L \times SU(3)_R$ hadronic model

The chiral $SU(3)_L \times SU(3)_R$ model has been successfully employed to analyze hadronic matter, finite-sized nuclei, hypernuclei, and neutron stars in which the baryonic chemical potential becomes large enough to produce particles beyond the lowest SU(2) multiplet of nucleons, including hyperons ($\Lambda, \Sigma^{\pm,0}, \Xi^{-,0}$) and other resonance states ($\Delta^{++,+,0,-}, \Sigma^{*\pm,0}, \Xi^{*0,-}, \Omega^-$). This model employs a flavor-SU(3) framework, incorporating octet and decuplet baryons along with strange mesons as fundamental elements within the primary hadronic SU(3) multiplets. The various terms of effective hadronic Lagrangian density of this model are given as

$$\mathcal{L} = \mathcal{L}_{\rm kin} + \mathcal{L}_{\rm int} + \mathcal{L}_{\rm scal} + \mathcal{L}_{\rm vec} + \mathcal{L}_{\rm SB}. \tag{1}$$

This equation arises from the relativistic quantum field theory of baryons and mesons, which incorporates essential QCD features, including broken scale invariance [45,128] and the nonlinear realization of chiral symmetry [129]. The term $\mathcal{L}_{\rm kin}$ in Eq. (1) is the kinetic energy term for different particles, and the term $\mathcal{L}_{\rm int}$ includes the interaction of baryons with various mesons. As discussed before, the interaction of octet and decuplet baryons is considered through the exchange of scalar fields, σ, ζ, and δ and vector fields, ω, ρ, and ϕ. Medium-range attractive interactions between hadrons are influenced by scalar fields, while vector fields affect short-range repulsive interactions. The interactions occurring between baryons via scalar mesonic fields are responsible for generating the baryon masses. This occurs through the coupling of baryons to two distinct scalar quark condensates: (i) the nonstrange σ, which is composed of up and down quarks ($\sim\langle\bar{u}u + \bar{d}d\rangle$), and (ii) the strange ζ, which is composed of strange quarks $\sim\langle\bar{s}s\rangle$. Additionally, to address the isospin asymmetry within the medium and the QCD trace anomaly properties, this model incorporates the scalar isovector field δ and the dilaton field χ, respectively. In Eq. (1), the third term $\mathcal{L}_{\rm scal}$ and the fourth term $\mathcal{L}_{\rm vec}$ of the Lagrangian density represent the self-interaction for scalar and vector mesons, respectively. The last term, $\mathcal{L}_{SB}$, corresponds to the explicit breaking of chiral symmetry, which serves to eliminate the Goldstone bosons. Detailed explanations of interaction Lagrangian density terms can be found in the literature [45,51,52].

To examine the properties of hadronic matter in a nonperturbative domain, we utilize the mean-field approximation. This method involves substituting the quantum field operator with their anticipated classical expectation values; i.e., $\Phi(x) = \langle\Phi\rangle + \delta\Phi \to \langle\Phi\rangle \equiv \Phi$ for scalar fields and $V_\mu(x) = \langle V\rangle\delta_{0\mu} + \delta V_\mu \to \langle V_0\rangle \equiv V$ for vector fields as these fields are expected to exhibit minimal fluctuations in high-density environments [45]. The thermodynamic potential per unit volume $\frac{\Omega}{V}$ for isospin asymmetric resonance medium is calculated under this approximation and is expressed by the following equation:

$$\frac{\Omega}{V} = -\frac{\gamma_i T}{(2\pi)^3}\sum_i \int d^3k\{\ln\left(1 + e^{-\beta[E_i^*(k)-\mu_i^*]}\right) + \ln\left(1 + e^{-\beta[E_i^*(k)+\mu_i^*]}\right)\} - \mathcal{L}_M - V_{\rm vac}. \tag{2}$$

Here, the summation is over the baryons of the medium, i.e., $i = p, n, \Lambda, \Sigma^{\pm,0}, \Xi^{-,0}, \Delta^{++,+,0,-}, \Sigma^{*\pm,0}, \Xi^{*0,-}, \Omega^-$. γ_i denotes the spin degeneracy factor, which equals 2 for octet baryons and 4 for decuplet baryons, and $\mathcal{L}_M = \mathcal{L}_{\rm vec} + \mathcal{L}_0 + \mathcal{L}_{SB}$. Also, $E_i^*(k) = \sqrt{k^2 + m_i^{*2}}$ and effective baryon mass, m_i^*, is calculated using relation

$$m_i^* = -(g_{\sigma i}\sigma + g_{\zeta i}\zeta + g_{\delta i}\tau_{3i}\delta) + m_{i0}, \tag{3}$$

where $g_{\sigma i}$, $g_{\zeta i}$, and $g_{\delta i}$ are couplings of σ, ζ, and δ fields, respectively, with different baryons and the term m_{i0} is fitted to obtain the baryon vacuum masses. Also, τ_{3i} has values $+1$ for $p, \Sigma^+, \Xi^0, \Delta^+, \Sigma^{*+}, \Xi^{*0}$, -1 for $n, \Sigma^-, \Xi^-, \Delta^0, \Sigma^{*-}, \Xi^{*-}$, 0 for $\Lambda, \Sigma^0, \Sigma^{*0}$, $+3$ for Δ^{++} and -3 for Δ^- baryons. The effective chemical potential of baryons is defined as $\mu_i^* = \mu_i - g_{\omega i}\omega - g_{\phi i}\phi - g_{\rho i}\tau_{3i}\rho$, where $g_{\omega i}$, $g_{\phi i}$, and $g_{\rho i}$ serve as the coupling constants between the baryons and ω, ϕ, and ρ fields, respectively. These vector coupling constants are adjusted to match nuclear saturation properties, such as the binding energy ($B/A = -16$ MeV) at $\rho_0 = 0.15$ fm^{-3} for symmetric nuclear matter. The term $V_{\rm vac}$ in Eq. (2) is subtracted to ensure that the vacuum energy is zero. Equation (2) is subjected to minimization with respect to the mesonic fields through the following relations:

$$\frac{\partial\Omega}{\partial\sigma} = \frac{\partial\Omega}{\partial\zeta} = \frac{\partial\Omega}{\partial\delta} = \frac{\partial\Omega}{\partial\chi} = \frac{\partial\Omega}{\partial\omega} = \frac{\partial\Omega}{\partial\rho} = \frac{\partial\Omega}{\partial\phi} = 0. \tag{4}$$

At finite values of baryon density ρ_B, temperature T, isospin asymmetry I_a, and strangeness fraction f_s of the medium, the nonlinear equations obtained through above relations for both the scalar and vector fields are solved. Additionally, the vector and scalar densities of the baryons, denoted by the symbols ρ_i^v and ρ_i^s, respectively, are expressed as

$$\rho_i^v = \gamma_i \int \frac{d^3k}{(2\pi)^3}\left(\frac{1}{1+\exp\left[\beta(E_i^*(k)-\mu_i^*)\right]} - \frac{1}{1+\exp\left[\beta(E_i^*(k)+\mu_i^*)\right]}\right) \tag{5}$$

and

$$\rho_i^s = \gamma_i \int \frac{d^3k}{(2\pi)^3}\frac{m_i^*}{E_i^*(k)}\left(\frac{1}{1+\exp\left[\beta(E_i^*(k)-\mu_i^*)\right]} + \frac{1}{1+\exp\left[\beta(E_i^*(k)+\mu_i^*)\right]}\right). \tag{6}$$

For the variables I_a and f_s, their definitions are $-\frac{\sum_i I_{3i}\rho_i^v}{\rho_B}$ and $\frac{\sum_i |S_i|\rho_i^v}{\rho_B}$, respectively, with ρ_B as the total baryonic density of the medium under consideration.

B. In-medium masses of K and $\bar{K}$ mesons

To evaluate ϕ meson properties, it is essential first to calculate in-medium kaon (antikaon) masses, which are influenced by how K ($\bar{K}$) interact with the surrounding resonance environment. In this section, we calculate medium-modified masses of kaons, K (K^+, K^0), and antikaons, $\bar{K}(K^-, \overline{K^0})$, in the isospin asymmetric dense resonance medium via the dispersion relation. The Lagrangian density that reflects the interaction of K ($\bar{K}$) with octet and decuplet baryons can be written as [52,130]

$$\mathcal{L}_{KB} = \mathcal{L}_{BW} + \mathcal{L}_{\rm mass} + \mathcal{L}_{\rm 1st\,range\ term} + \mathcal{L}_{d_1}^{BM} + \mathcal{L}_{d_2}^{BM}. \tag{7}$$

The first term, $\mathcal{L}_{BW}$, is described as a vectorial interaction term, which is derived from the kinetic term of interaction Lagrangian of Eq. (1) and can be expressed as $\mathcal{L}_{\rm BW} = i{\rm Tr}(\bar{B}\gamma^\mu D_\mu B) - i\bar{T}^\mu \not{D} T_\mu$, where B and T^μ are octet and decuplet baryon fields, respectively and D_μ denotes covariant derivative. The second term is a mass term, which originates from explicit symmetry breaking, while the third term is a result of the kinetic terms of pseudoscalar mesons in the chiral effective Lagrangian. The $\mathcal{L}_{d_1}^{BM}$ and $\mathcal{L}_{d_2}^{BM}$ terms are referred to as range terms, obtained from the chiral model's baryon-meson interaction Lagrangian [130,131]. Equation (7) can be expanded to the following [52,130]:

$$\mathcal{L}_{KB} = -\frac{i}{4f_K^2}[(2\bar{p}\gamma^\mu p + \bar{n}\gamma^\mu n - \overline{\Sigma^-}\gamma^\mu\Sigma^- + \overline{\Sigma^+}\gamma^\mu\Sigma^+ - 2\overline{\Xi^-}\gamma^\mu\Xi^- - \overline{\Xi^0}\gamma^\mu\Xi^0 + 3(3\overline{\Delta^{++}}\gamma^\mu\Delta^{++} + 2\overline{\Delta^+}\gamma^\mu\Delta^+ + \overline{\Delta^0}\gamma^\mu\Delta^0 - \overline{\Sigma^{*-}}\gamma^\mu\Sigma^{*-} + \overline{\Sigma^{*+}}\gamma^\mu\Sigma^{*+}$$

$$
\begin{aligned}
&- 2\overline{\Xi^{*-}}\gamma^{\mu}\Xi^{*-} - \overline{\Xi^{*0}}\gamma^{\mu}\Xi^{*0} - 3\overline{\Omega^{-}}\gamma^{\mu}\Omega^{-}))(K^{-}(\partial_{\mu}K^{+}) - (\partial_{\mu}K^{-})K^{+}) \\
&+ (\bar{p}\gamma^{\mu}p + 2\bar{n}\gamma^{\mu}n + \overline{\Sigma^{-}}\gamma^{\mu}\Sigma^{-} - \overline{\Sigma^{+}}\gamma^{\mu}\Sigma^{+} - \overline{\Xi^{-}}\gamma^{\mu}\Xi^{-} - 2\overline{\Xi^{0}}\gamma^{\mu}\Xi^{0} \\
&+ 3(3\overline{\Delta^{-}}\gamma^{\mu}\Delta^{-} + \overline{\Delta^{+}}\gamma^{\mu}\Delta^{+} + 2\overline{\Delta^{0}}\gamma^{\mu}\Delta^{0} - \overline{\Sigma^{*+}}\gamma^{\mu}\Sigma^{*+} + \overline{\Sigma^{*-}}\gamma^{\mu}\Sigma^{*-} \\
&- \overline{\Xi^{*-}}\gamma^{\mu}\Xi^{*-} - 2\overline{\Xi^{*0}}\gamma^{\mu}\Xi^{*0} - 3\overline{\Omega^{-}}\gamma^{\mu}\Omega^{-}))(\overline{K^{0}}(\partial_{\mu}K^{0}) - (\partial_{\mu}\overline{K^{0}})K^{0})] \\
&+ \frac{m_K^2}{2f_K}[(\sigma + \sqrt{2}\zeta + \delta)K^{+}K^{-} + (\sigma + \sqrt{2}\zeta - \delta)K^{0}\overline{K^{0}}] \\
&- \frac{1}{f_K}[(\sigma + \sqrt{2}\zeta + \delta)(\partial_{\mu}K^{+})(\partial^{\mu}K^{-}) + (\sigma + \sqrt{2}\zeta - \delta)(\partial_{\mu}K^{0})(\partial^{\mu}\overline{K^{0}})] \\
&+ \frac{d_1}{2f_K^2}[(\bar{p}p + \bar{n}n + \overline{\Lambda^{0}}\Lambda^{0} + \overline{\Sigma^{+}}\Sigma^{+} + \overline{\Sigma^{0}}\Sigma^{0} + \overline{\Sigma^{-}}\Sigma^{-} + \overline{\Xi^{-}}\Xi^{-} + \overline{\Xi^{0}}\Xi^{0} + 3(\overline{\Delta^{++}}\Delta^{++} \\
&+ \overline{\Delta^{+}}\Delta^{+} + \overline{\Delta^{-}}\Delta^{-} + \overline{\Delta^{0}}\Delta^{0} + \overline{\Sigma^{*+}}\Sigma^{*+} + \overline{\Sigma^{*0}}\Sigma^{*0} + \overline{\Sigma^{*-}}\Sigma^{*-} + \overline{\Xi^{*-}}\Xi^{*-} + \overline{\Xi^{*0}}\Xi^{*0} + \overline{\Omega^{-}}\Omega^{-})) \\
&\times ((\partial_{\mu}K^{+})(\partial^{\mu}K^{-}) + (\partial_{\mu}K^{0})(\partial^{\mu}\overline{K^{0}}))] \\
&+ \frac{d_2}{2f_K^2}\Bigg[\Bigg(\bar{p}p + \frac{5}{6}\overline{\Lambda^{0}}\Lambda^{0} + \frac{1}{2}\overline{\Sigma^{0}}\Sigma^{0} + \overline{\Sigma^{+}}\Sigma^{+} + \overline{\Xi^{-}}\Xi^{-} + \overline{\Xi^{0}}\Xi^{0} + 3\Bigg(\overline{\Delta^{++}}\Delta^{++} + \frac{2}{3}\overline{\Delta^{+}}\Delta^{+} \\
&+ \frac{1}{3}\overline{\Delta^{0}}\Delta^{0} + \overline{\Sigma^{*+}}\Sigma^{*+} + \frac{2}{3}\overline{\Sigma^{*0}}\Sigma^{*0} + \frac{1}{3}\overline{\Sigma^{*-}}\Sigma^{*-} + \frac{2}{3}\overline{\Xi^{*-}}\Xi^{*-} + \overline{\Xi^{*0}}\Xi^{*0} + \overline{\Omega^{-}}\Omega^{-}\Bigg)\Bigg)(\partial_{\mu}K^{+})(\partial^{\mu}K^{-}) \\
&+ \Bigg(\bar{n}n + \frac{5}{6}\overline{\Lambda^{0}}\Lambda^{0} + \frac{1}{2}\overline{\Sigma^{0}}\Sigma^{0} + \overline{\Sigma^{-}}\Sigma^{-} + \overline{\Xi^{-}}\Xi^{-} + \overline{\Xi^{0}}\Xi^{0} + 3\Bigg(\frac{1}{3}\overline{\Delta^{+}}\Delta^{+} + \frac{2}{3}\overline{\Delta^{0}}\Delta^{0} + \overline{\Delta^{-}}\Delta^{-} \\
&+ \frac{1}{3}\overline{\Sigma^{*+}}\Sigma^{*+} + \frac{2}{3}\overline{\Sigma^{*0}}\Sigma^{*0} + \overline{\Sigma^{*-}}\Sigma^{*-} + \frac{2}{3}\overline{\Xi^{*0}}\Xi^{*0} + \overline{\Xi^{*-}}\Xi^{*-} + \overline{\Omega^{-}}\Omega^{-}\Bigg)\Bigg)(\partial_{\mu}K^{0})(\partial^{\mu}\overline{K^{0}})\Bigg]. \qquad (8)
\end{aligned}
$$

In the above, the parameters d_1 and d_2 are assigned values of $2.56/m_K$ and $0.73/m_K$, respectively [130,131]. These values were determined by fitting to experimental measurements of the kaon-nucleon scattering length [132]. Using the Euler -Lagrangian equation of motion and applying Fourier transformation, the dispersion relations are obtained from Eq. (8) to calculate the medium-modified masses of K (K^+, K^0) and $\bar{K}$ (K^-, $\overline{K^0}$) mesons. Therefore, we have

$$
-\omega^2 + \vec{k}^2 + m^2_{K(\bar{K})} - \Pi^*(\omega, |\vec{k}|) = 0, \qquad (9)
$$

where the in-medium self-energy for K and $\bar{K}$ mesons is represented by $\Pi^*(\omega, |\vec{k}|)$. The kaon isospin doublet K (K^+, K^0) has its self-energy expressed as

$$
\begin{aligned}
\Pi^*_K(\omega, |\vec{k}|) = &-\frac{1}{4f_K^2}[3(\rho_p + \rho_n) \pm (\rho_p - \rho_n) \pm 2(\rho_{\Sigma^+} - \rho_{\Sigma^-}) - (3(\rho_{\Xi^-} + \rho_{\Xi^0}) \pm (\rho_{\Xi^-} \\
&- \rho_{\Xi^0})) + 3\{(3(\rho_{\Delta^+} + \rho_{\Delta^0}) \pm (\rho_{\Delta^+} - \rho_{\Delta^0})) \pm 2(\rho_{\Sigma^{*+}} - \rho_{\Sigma^{*-}}) \\
&- (3(\rho_{\Xi^{*-}} + \rho_{\Xi^{*0}}) \pm (\rho_{\Xi^{*-}} - \rho_{\Xi^{*0}})) - 6\rho_{\Omega^-} + 6(a\rho_{\Delta^{++}} + b\rho_{\Delta^-})\}]\omega \\
&+ \frac{m_K^2}{2f_K}(\sigma' + \sqrt{2}\zeta' \pm \delta') \\
&+ \Bigg[-\frac{1}{f_K}(\sigma' + \sqrt{2}\zeta' \pm \delta') + \frac{d_1}{2f_K^2}(\rho^s{}_p + \rho^s{}_n + \rho^s{}_{\Lambda^0} + \rho^s{}_{\Sigma^+} + \rho^s{}_{\Sigma^0} + \rho^s{}_{\Sigma^-} \\
&+ \rho^s{}_{\Xi^-} + \rho^s{}_{\Xi^0} + 3\{\rho^s{}_{\Delta^{++}} + \rho^s{}_{\Delta^+} + \rho^s{}_{\Delta^0} + \rho^s{}_{\Delta^-} + \rho^s{}_{\Sigma^{*+}} + \rho^s{}_{\Sigma^{*0}} + \rho^s{}_{\Sigma^{*-}} \\
&+ \rho^s{}_{\Xi^{*-}} + \rho^s{}_{\Xi^{*0}} + \rho^s{}_{\Omega^-}\}) + \frac{d_2}{4f_K^2}\Bigg((\rho^s{}_p + \rho^s{}_n) \pm (\rho^s{}_p - \rho^s{}_n) + \rho^s{}_{\Sigma^0} + \frac{5}{3}\rho^s{}_{\Lambda^0} \\
&+ (\rho^s{}_{\Sigma^+} + \rho^s{}_{\Sigma^-}) \pm (\rho^s{}_{\Sigma^+} - \rho^s{}_{\Sigma^-}) + 2\rho^s{}_{\Xi^-} + 2\rho^s{}_{\Xi^0} + 3\Bigg\{2(a\rho^s{}_{\Delta^{++}} + b\rho^s{}_{\Delta^-}) \qquad (10)
\end{aligned}
$$

$$+\frac{1}{3}(3(\rho^s_{\Delta^+}+\rho^s_{\Delta^0})\pm(\rho^s_{\Delta^+}-\rho^s_{\Delta^0}))+\frac{4}{3}\rho^s_{\Sigma^{*0}}+\frac{1}{3}(4(\rho^s_{\Sigma^{*+}}+\rho^s_{\Sigma^{*-}})\pm 2(\rho^s_{\Sigma^{*+}}-\rho^s_{\Sigma^{*-}}))$$
$$+\frac{1}{3}(5(\rho^s_{\Xi^{*0}}+\rho^s_{\Xi^{*-}})\pm(\rho^s_{\Xi^{*0}}-\rho^s_{\Xi^{*-}}))+2\rho^s_{\Omega^-}\Big\}\Big)\Big](\omega^2-\vec{k}^2).$$

The symbols σ', ζ', and δ' represent the variations of the σ, ζ, and δ fields from their corresponding vacuum expectation values, which are symbolized as σ_0, ζ_0, and δ_0. The following expression is derived for the self-energy of antikaon isospin doublet $\bar{K}$ (K^-, $\overline{K^0}$):

$$\begin{aligned}\Pi^*_{\bar{K}}(\omega,|\vec{k}|)=&\frac{1}{4f_K^2}[3(\rho_p+\rho_n)\pm(\rho_p-\rho_n)\pm 2(\rho_{\Sigma^+}-\rho_{\Sigma^-})-(3(\rho_{\Xi^-}+\rho_{\Xi^0})\pm(\rho_{\Xi^-}\\&-\rho_{\Xi^0}))+3\{(3(\rho_{\Delta^+}+\rho_{\Delta^0})\pm(\rho_{\Delta^+}-\rho_{\Delta^0}))\pm 2(\rho_{\Sigma^{*+}}-\rho_{\Sigma^{*-}})\\&-(3(\rho_{\Xi^{*-}}+\rho_{\Xi^{*0}})\pm(\rho_{\Xi^{*-}}-\rho_{\Xi^{*0}}))-6\rho_{\Omega^-}+6(a\rho_{\Delta^{++}}+b\rho_{\Delta^-})\}]\omega\\&+\frac{m_K^2}{2f_K}(\sigma'+\sqrt{2}\zeta'\pm\delta')\\&+\Bigg[-\frac{1}{f_K}(\sigma'+\sqrt{2}\zeta'\pm\delta')+\frac{d_1}{2f_K^2}(\rho^s{}_p+\rho^s{}_n+\rho^s{}_{\Lambda^0}+\rho^s{}_{\Sigma^+}+\rho^s{}_{\Sigma^0}+\rho^s{}_{\Sigma^-}\\&+\rho^s{}_{\Xi^-}+\rho^s{}_{\Xi^0}+3\{\rho^s{}_{\Delta^{++}}+\rho^s{}_{\Delta^+}+\rho^s{}_{\Delta^0}+\rho^s{}_{\Delta^-}+\rho^s{}_{\Sigma^{*+}}+\rho^s{}_{\Sigma^{*0}}+\rho^s{}_{\Sigma^{*-}}\\&+\rho^s{}_{\Xi^{*-}}+\rho^s{}_{\Xi^{*0}}+\rho^s{}_{\Omega^-}\})+\frac{d_2}{4f_K^2}\Bigg((\rho^s{}_p+\rho^s{}_n)\pm(\rho^s{}_p-\rho^s{}_n)+\rho^s{}_{\Sigma^0}+\frac{5}{3}\rho^s{}_{\Lambda^0}\\&+(\rho^s{}_{\Sigma^+}+\rho^s{}_{\Sigma^-})\pm(\rho^s{}_{\Sigma^+}-\rho^s{}_{\Sigma^-})+2\rho^s{}_{\Xi^-}+2\rho^s{}_{\Xi^0}+3\{2(a\rho^s_{\Delta^{++}}+b\rho^s_{\Delta^-})\\&+\frac{1}{3}(3(\rho^s_{\Delta^+}+\rho^s_{\Delta^0})\pm(\rho^s_{\Delta^+}-\rho^s_{\Delta^0}))+\frac{4}{3}\rho^s_{\Sigma^{*0}}+\frac{1}{3}(4(\rho^s_{\Sigma^{*+}}+\rho^s_{\Sigma^{*-}})\pm 2(\rho^s_{\Sigma^{*+}}-\rho^s_{\Sigma^{*-}}))\\&+\frac{1}{3}(5(\rho^s_{\Xi^{*0}}+\rho^s_{\Xi^{*-}})\pm(\rho^s_{\Xi^{*0}}-\rho^s_{\Xi^{*-}}))+2\rho^s_{\Omega^-}\}\Bigg)\Bigg](\omega^2-\vec{k}^2).\end{aligned}\tag{11}$$

In the previously mentioned equations, the $\pm$ sign gives $\Pi^*_{K^+}$ ($\Pi^*_{K^-}$) and $\Pi^*_{K^0}$ ($\Pi^*_{\bar{K}^0}$), respectively. The parameters are assigned as $a=1$, $b=0$ for K^+ and K^-, but $a=0$ and $b=1$ are used for K^0 and $\bar{K}^0$. The in-medium masses of $K(\bar{K})$ mesons in the dense resonance matter are determined at momentum $|\vec{k}|=0$ using Eq. (9) with m_K and $m_{\bar{K}}$ denoting the vacuum masses of kaons and antikaons, respectively.

C. In-medium mass and decay width of ϕ meson

The in-medium masses of K and $\bar{K}$ mesons calculated in the isospin asymmetric resonance medium are used as input in the current subsection to compute the in-medium properties of ϕ for the decay channel $\phi\to K\bar{K}$ at one-loop level as depicted in Fig. 1. The interaction Lagrangian density for coupling of ϕ meson to $K\bar{K}$ is given as [133,134]

$$\mathcal{L}_{\phi K\bar{K}}=ig_\phi\phi^\mu[\bar{K}(\partial_\mu K)-(\partial_\mu\bar{K})K].\tag{12}$$

The present study has not taken into account the $\phi\phi K\bar{K}$ interactions, as their impact on in-medium masses and decay width of ϕ meson is minimal compared to the $\phi K\bar{K}$ interactions [88]. The scalar part of the in-medium self-energy corresponding to the loop diagram for ϕ meson at rest can be expressed as

$$i\Pi^*_\phi(p)=-\frac{8}{3}g_\phi^2\int\frac{d^4q}{(2\pi)^4}\vec{q}^2D_K(q)D_{\bar{K}}(q-p).\tag{13}$$

In the above, $D_K(q)=(q^2-m_K^{*^2}+i\epsilon)^{-1}$ and $D_{\bar{K}}(q-p)=((q-p)^2-m_{\bar{K}}^{*^2}+i\epsilon)^{-1}$ represent the kaon and antikaon propagators, respectively. The ϕ meson four-momentum vector is denoted by $p=(p^0=m^*_\phi,\vec{0})$, with m^*_ϕ indicating the in-medium mass of the ϕ meson. The average masses of

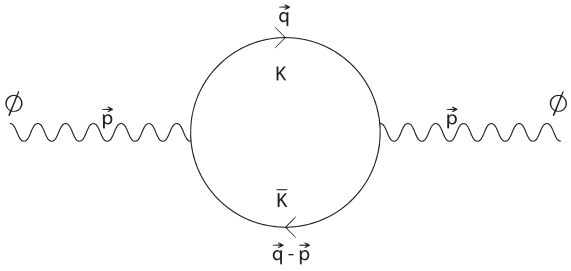


FIG. 1. $\phi K\bar{K}$ interaction at one-loop level.

kaon and antikaon are symbolized by $m_K^*(=\frac{m_{K^+}^*+m_{K^0}^*}{2})$ and $m_{\bar{K}}^*(=\frac{m_{K^-}^*+m_{\bar{K}^0}^*}{2})$, respectively. Values of $m_{K^+}^*$, $m_{K^0}^*$, $m_{K^-}^*$, and $m_{\bar{K}^0}^*$ are calculated by using Eq. (9) for finite T, I_a, and f_s within the medium. The effective mass of the ϕ meson is calculated from the real part of $\Pi_\phi^*(p)$ through relation [88]

$$m_\phi^{*^2} = (m_\phi^0)^2 + \mathrm{Re}\Pi_\phi^*(m_\phi^{*^2}), \tag{14}$$

where m_ϕ^0 is the bare mass of the ϕ meson. The real part of self-energy is given as [48,88]

$$\mathrm{Re}\Pi_\phi^* = -\frac{4}{3}g_\phi^2\mathcal{P}\int\frac{d^3q}{(2\pi)^3}\vec{q}^2\frac{(E_K^*+E_{\bar{K}}^*)}{E_K^*E_{\bar{K}}^*((E_K^*+E_{\bar{K}}^*)^2-m_\phi^{*^2})}, \tag{15}$$

where $E_{K/\bar{K}}^* = (\vec{q}^2 + m_{K/\bar{K}}^{*^2})^{1/2}$ and $\mathcal{P}$ stands for principal value of the integral. The integral in Eq. (15) exhibits divergence but must be regularized. To address this, we employ a phenomenological vertex form factor that incorporates a cutoff parameter Λ_c as in Ref. [135]. The loop integral after renormalization is expressed as

$$\mathrm{Re}\Pi_\phi^* = -\frac{4}{3}g_\phi^2\mathcal{P}\int_0^{\Lambda_c}\frac{d^3q}{(2\pi)^3}\vec{q}^2\left(\frac{\Lambda_c^2+m_\phi^{*^2}}{\Lambda_c^2+4E_K^{*^2}}\right)^4 \times\frac{(E_K^*+E_{\bar{K}}^*)}{E_K^*E_{\bar{K}}^*((E_K^*+E_{\bar{K}}^*)^2-m_\phi^{*^2})}. \tag{16}$$

Thermal behavior of the ϕ meson at one-loop order has been explored in Refs. [136–138] considering Matsubara formalism. However, in our present manuscript, the impact of finite temperature is incorporated through the grand thermodynamic potential given in Eq. (2) of the chiral SU(3) model. This temperature dependence dynamically influences the in-medium scalar and vector meson fields which are obtained by solving the coupled system of nonlinear equations [see Eq. (4)]. The expressions of vector and scalar densities of baryons [Eqs. (5) and (6)] defined at finite temperature will enter in the equations of motion of vector and scalar fields, respectively. Temperature-dependent scalar fields and also the values of scalar and vector densities of baryons are used to calculate the medium-modified effective masses of the kaons and antikaons using dispersion relation given in Eq. (9). These effective K ($\bar{K}$) masses calculated at finite temperature are then employed as input in the one-loop ϕ meson self-energy calculations, effectively capturing medium effects in a thermodynamically consistent manner. More explicit calculations considering temperature dependence in the kaon-antikaon loop through Matsubara formalism will be done in the future. By using a quark pair creation model and applying the Gaussian wave function of mesons, the vertex form factor can be calculated to get a rough approximation of Λ_c [48,135,139,140]. The study in Ref. [135] calculated the in-medium masses of J/ψ using vertex form factors, with Λ_c values vary in the range $1 \leq \Lambda_c \leq 3$ GeV. A comparable range for Λ_c (1 to 4 GeV) was employed to determine the masses of ϕ meson within hadronic medium in Refs. [48,88]. Thus, we consider values of Λ_c in the range 2 to 4 GeV to understand its impact on the properties of the ϕ meson in isospin asymmetric resonance medium. The decay width of the ϕ meson is derived from the imaginary component of the self-energy $\mathrm{Im}\,\Pi_\phi^*$ and given as [141]

$$\Gamma_\phi^* = \frac{g_\phi^2}{24\pi}\frac{1}{m_\phi^{*^5}}((m_\phi^{*^2}-(m_K^*+m_{\bar{K}}^*)^2)(m_\phi^{*^2}-(m_K^*-m_{\bar{K}}^*)^2))^{3/2}. \tag{17}$$

In the vacuum, the empirical width of the ϕ meson is used to calculate the coupling constant g_ϕ, which is 4.539 in this work.

III. RESULTS AND DISCUSSION

In this section, we discuss the results of in-medium properties of K, $\bar{K}$, and ϕ mesons in the dense resonance medium. We mainly examine the impact of baryonic density ρ_B, temperatures T, isospin asymmetry I_a, and strangeness fraction f_s of the resonance medium on the medium-modified mass and decay width of ϕ meson. The coupling constants that reflect the strength of interaction of scalar and vector fields with baryons as well as the baryonic potential, U_i, are presented in Table I. The parameter m_3^i is fitted to reproduce the reasonable baryonic potential through the relation, $U_i = M_i^* - m_i + g_{\omega i}\omega + g_{\rho i}\tau_{3i}\rho + g_{\phi i}\phi$, where $M_i^* = m_i^* + m_3^i(\sqrt{2}(\sigma-\sigma_0)+(\zeta-\zeta_0))$ at nuclear saturation density for symmetric nuclear matter. The other parameters of the chiral SU(3) hadronic mean-field model are specified as follows: $k_0 = 2.37$, $k_1 = 1.40$, $k_2 = -5.55$, $k_3 = -2.65$, $k_4 = -0.23$, $g_4 = 38.9$, $d = 0.06$, $m_\pi = 139$ MeV, pion decay constant $f_\pi = 93.3$ MeV, $m_K = 498$ MeV, and the kaon decay constant $f_K = 122$ MeV. The vacuum values for the scalar fields are $\sigma_0 = -93.3$ MeV, $\zeta_0 = -106.76$ MeV, and $\chi_0 = 401.91$ MeV.

A. In-medium mass of kaon and antikaon in resonance matter

In this subsection, we discuss the results of medium-modified kaon and antikaon masses in isospin asymmetric resonance matter at finite density and temperature. To compute the in-medium properties of the ϕ meson, it is essential first to determine in-medium K ($\bar{K}$) masses as detailed in Refs. [48,88]. The chiral SU(3) model is employed to calculate effective K ($\bar{K}$) masses by utilizing medium-modified scalar fields (σ, ζ, and δ) along with vector and scalar baryonic densities, as described in self-energy expressions given in Eqs. (10) and (11). Our

TABLE I. Different coupling constants, parameter m_3^i and the baryonic potential U_i used in present calculations.

Baryon	m_i (MeV)	$g_{\sigma i}$	$g_{\zeta i}$	$g_{\delta i}$	$g_{\omega i}$	$g_{\rho i}$	$g_{\phi i}$	m_3^i	U_i (MeV)
N	939	9.83	−1.22	2.34	11.8	4.7	0	−0.11	−71
Λ	1115	5.31	5.80	0	8.89	0	−6.29	0.44	−28
Σ	1193	6.13	5.80	6.79	8.89	8.89	−6.28	2.12	30
Ξ	1315	3.68	9.14	2.36	4.44	4.44	−12.56	1.6	−18
Δ	1232	10.74	2.20	2.49	12.74	12.74	0	0.68	−80
Σ^*	1385	8.20	5.80	3.47	8.50	8.50	−6.01	1.45	−64
Ξ^*	1530	5.66	9.40	2.34	4.25	4.25	−12.01	1.28	−19
Ω	1672	3.12	15.19	0	0	0	−18.02	3.44	−25

previous study [52] discussed how the presence of resonance baryons in the medium leads to significant modifications in the effective masses of K (K^+, K^0) and $\bar{K}$ ($\bar{K}^0$, $\bar{K}^0$). In the present study, the average kaon mass, $m_K^* = \frac{m_{K^+}^* + m_{K^0}^*}{2}$, and antikaon mass, $m_{\bar{K}}^* = \frac{m_{\bar{K}^0}^* + m_{\bar{K}^0}^*}{2}$, represented in Figs. 2 and 3, are utilized to determined the in-medium mass of ϕ meson. These figures illustrate the 3D representation of the effective mass of kaon (m_K^*) and antikaon ($m_{\bar{K}}^*$) plotted with respect to baryonic density ratio ρ_B/ρ_0 and temperature T in dense resonance matter for isospin asymmetry $I_a = 0$ and 0.3 and strangeness fractions $f_s = 0$ and 0.5.

In Fig. 2(a), we consider a symmetric medium ($I_a = 0$), comprising of nonstrange particles (p, n, and $\Delta^{++,+,0,-}$),

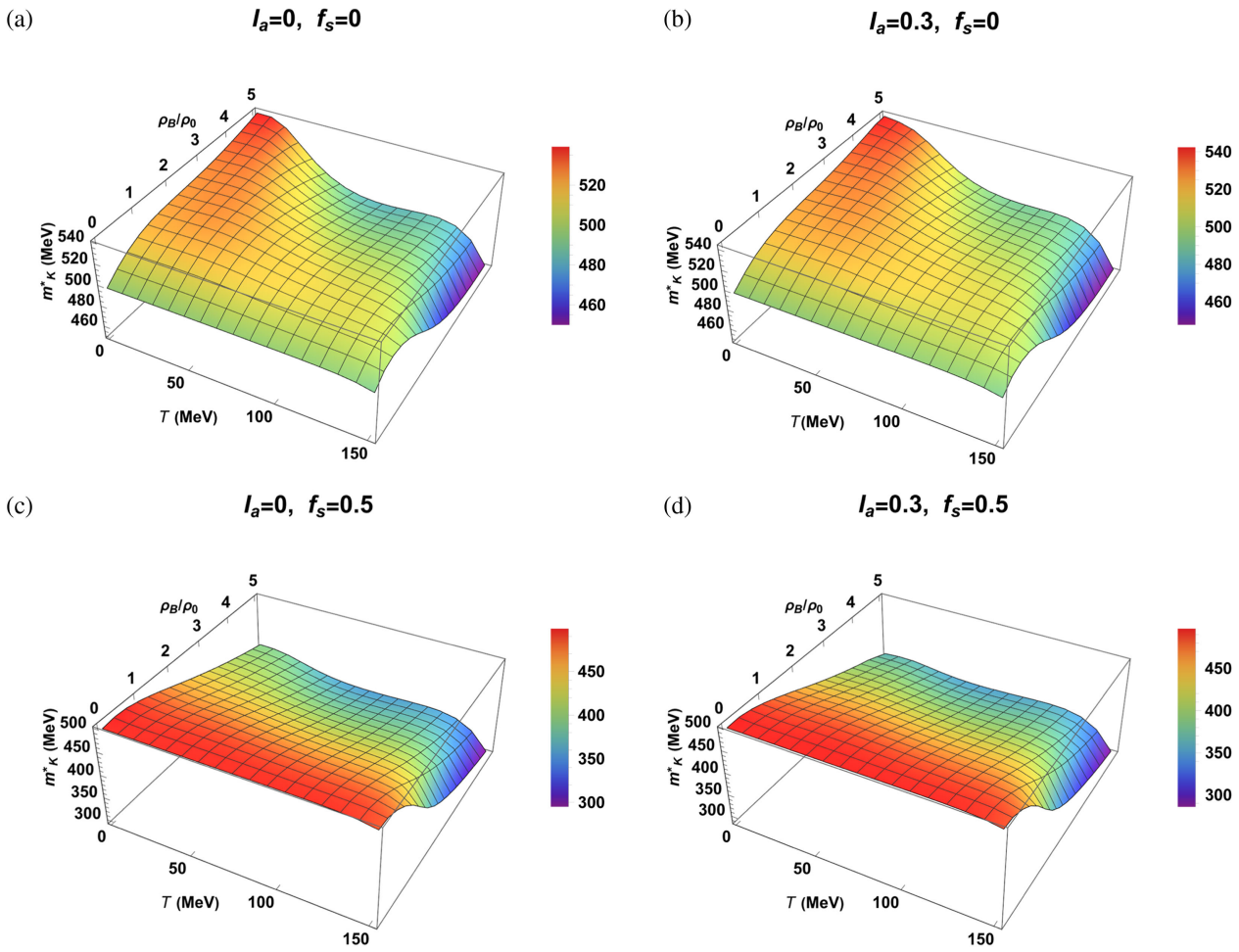


FIG. 2. The average effective kaon mass m_K^* is plotted for resonance medium as a function of baryonic density ratio ρ_B/ρ_0 and temperature T under various conditions of isospin asymmetry parameter I_a and strangeness fraction f_s of the medium. For each value of the isospin asymmetry parameter ($I_a = 0$ and 0.3), the results are shown for $f_s = 0$ [in the subplots (a) and (b)] and $f_s = 0.5$ [in subplots (c) and (d)].

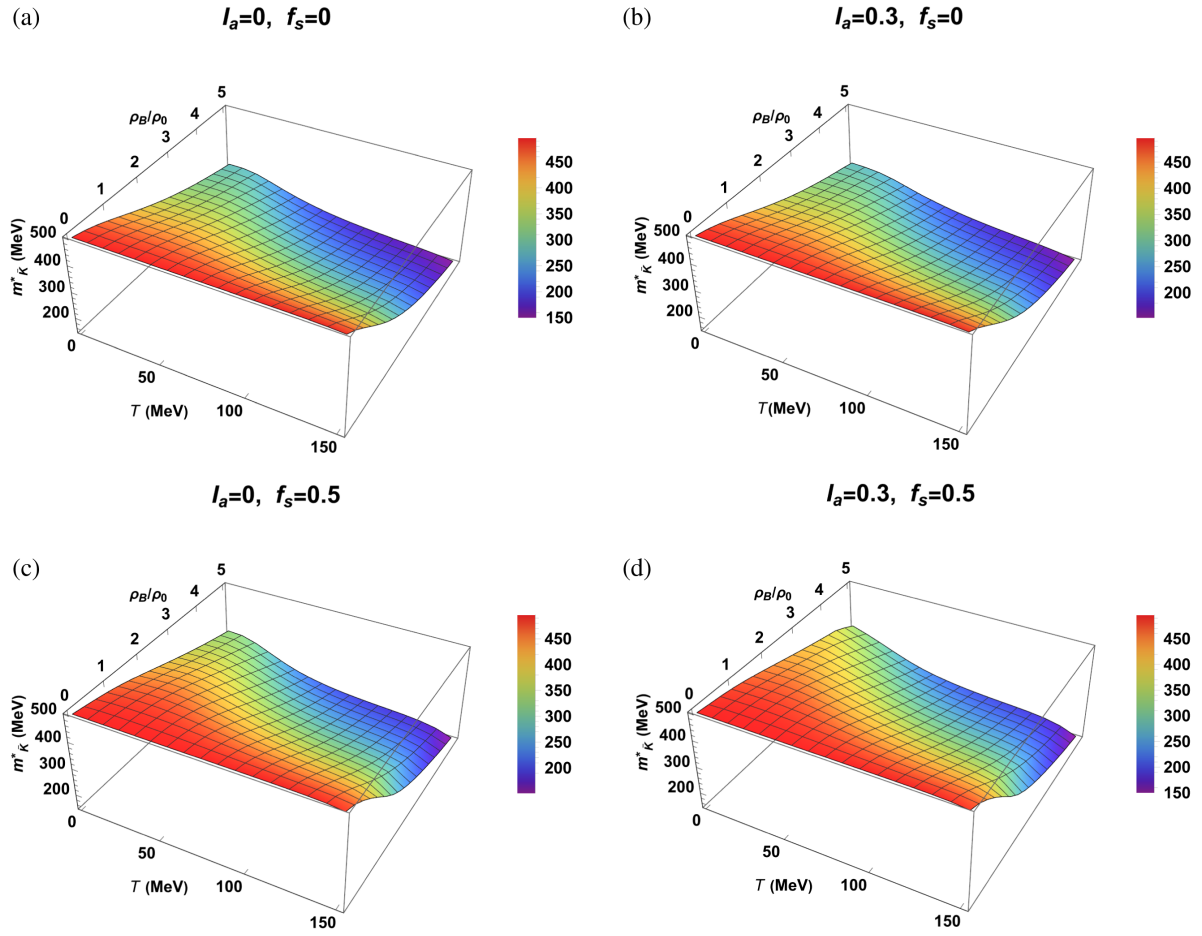


FIG. 3. The average effective antikaon mass $m^*_{\bar{K}}$ is plotted for resonance medium with respect to the baryonic density ratio ρ_B/ρ_0 and temperature T. For each value of the isospin asymmetry parameter ($I_a = 0$ and 0.3), the results are shown for $f_s = 0$ [in the subplots (a) and (b)] and $f_s = 0.5$ [in subplots (c) and (d)].

i.e., $f_s = 0$ case. At lower temperature, the effective kaon mass is observed to increase as baryonic density rises from zero to $5\rho_0$, while at higher temperature, the opposite trend is observed with an increase in ρ_B/ρ_0 as exhibited in Fig. 2(a). The effective masses of K and $\bar{K}$ mesons in the chiral SU(3) model are evaluated by incorporating the effects of various interaction terms into the total Lagrangian density, as specified in Eq. (7). Among the interaction terms in this Lagrangian, the vectorial interaction term has a significant impact on m^*_K, causing a repulsive influence at low temperatures and an attractive effect at high temperatures. In Fig. 2(b), for asymmetric medium with $I_a = 0.3$, where a comparable trend is observed as in Fig. 2(a), the change in magnitude of m^*_K from its vacuum value (496 MeV) as a function of ρ_B and T increases slightly. The incorporation of strange particles within the medium at a given temperature, where all spin-$\frac{1}{2}$ octet $(p, n, \Lambda, \Sigma^{\pm,0}, \Xi^{-,0})$ as well as spin-$\frac{3}{2}$ decuplet $(\Delta^{++,+,0,-}, \Sigma^{*\pm,0}, \Xi^{*0,-}, \Omega^-)$ baryons are considered, leads to a decrease in the effective mass of K mesons due to dominant attractive interactions between kaons and baryons, as represented in Figs. 2(c) and 2(d). As can be seen from these results, the m^*_K decreases with respect to baryonic density at lower temperature. However, at higher temperature, the rate of drop of kaon mass is more noticeable as shown in Figs. 2(c) and 2(d). Similar to kaon masses, antikaon masses are plotted in Fig. 3, and their respective results show the reduction in $m^*_{\bar{K}}$ with variation in temperature and baryonic density, regardless of values of I_a and f_s. A comparison of Figs. 2 and 3 reveal a more sizable reduction in antikaon masses compared to kaons at higher temperatures and densities.

B. In-medium mass of ϕ meson in resonance medium

Next, we extend our numerical analysis to the in-medium ϕ meson properties in isospin asymmetric resonance matter. In Refs. [88,89], the ϕ meson self-energy in cold nuclear matter is calculated by employing quark-meson coupling model under simplifying assumption $m^*_K = m^*_{\bar{K}}$. However, Refs. [48,49] and the current study treat these meson masses differently, i.e., $m^*_K \neq m^*_{\bar{K}}$ at finite temperature. To determine the medium-modified ϕ meson mass

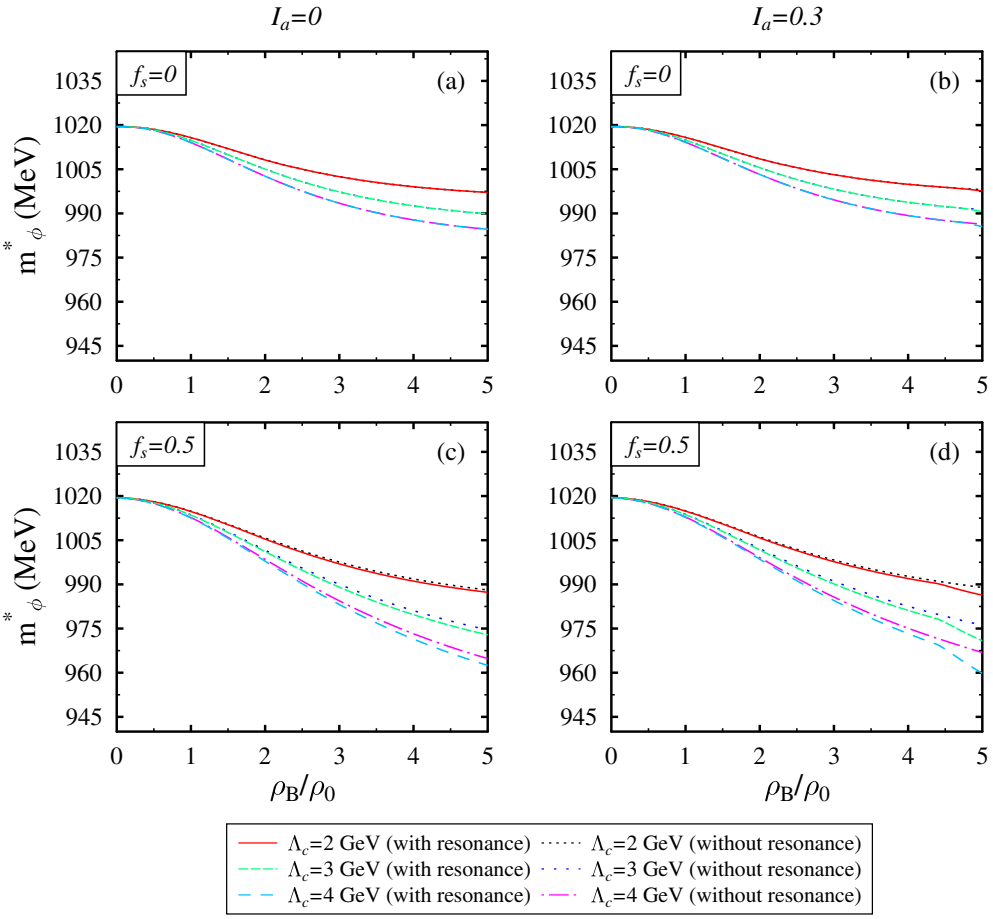


FIG. 4. The comparison of m^*_ϕ in resonance and non-resonance matter as a function of baryon density ratio ρ_B/ρ_0 for different values of Λ_c, I_a, and f_s at temperature $T = 0$ MeV. The results corresponding to isospin asymmetry parameters $I_a = 0$ and 0.3 are displayed for the strangeness fractions $f_s = 0$ in subplots (a) and (b), and $f_s = 0.5$ in subplots (c) and (d).

within the resonance medium, we plugged the findings of kaon and antikaon energies into Eq. (15), the real part of the self-energy of the ϕ meson. In Figs. 4 and 5, the behavior of ϕ meson mass in isospin asymmetric dense resonance matter is analyzed by plotting it with respect to the baryon density ratio ρ_B/ρ_0 (in units of nuclear saturation density ρ_0) for different values of cutoff mass parameter Λ_c, at temperatures $T = 0$ and 100 MeV, respectively. In each subplot, our results are presented for the scenarios that consider calculations with and without including decuplet baryons. The values of effective masses of ϕ mesons are tabulated at specific values of Λ_c, ρ_B, I_a, f_s, and T in Table II. In Figs. 4(a) and 4(b), at $f_s = 0$, considering nucleons and Δ baryons, the magnitude of m^*_ϕ decreases significantly with increasing the value of Λ_c for both the symmetric ($I_a = 0$) and asymmetric ($I_a = 0.3$) resonance media. However, the reduction in m^*_ϕ with respect to Λ_c is slightly less noticeable in the asymmetric matter across all ρ_B values. We also observed that at $T = 0$ the effective mass of ϕ meson almost remains the same for both pure nuclear matter and Δ resonance matter, i.e., regardless of the presence or absence of resonance decuplets, up to the considered ρ_B/ρ_0 ratio in this study, as depicted in Figs. 4(a) and 4(b). This consistency is attributed to the fact that Δ baryons are populated at higher baryonic densities, as elaborated in our previous investigation [52].

As we shift to a strange medium where $f_s = 0.5$, it is noticed that m^*_ϕ exhibits similar behavior in both media (with and without resonance) as the function of ρ_B/ρ_0 ratio as well as Λ_c, as can be seen in Figs. 4(c) and 4(d). In a medium containing only hyperons, as the value of cutoff parameter Λ_c increases, the m^*_ϕ curve shifts downward. However, when decuplets are incorporated into this medium, the same trend is observed with a more remarkable reduction in m^*_ϕ as Λ_c increases for all baryonic densities due to dominant attractive interactions. This significant reduction in m^*_ϕ reflects the medium-modified mass behavior of kaon (antikaon) in these environments. With the increase in temperature, $T = 100$ MeV, a more pronounced reduction in m^*_ϕ is observed with increasing density and Λ_c as compared to $T = 0$ MeV, as shown in Fig. 5. At $T = 0$ and 100 MeV, in the non-strange ($f_s = 0$) isospin asymmetric ($I_a = 0.3$) resonance medium, at

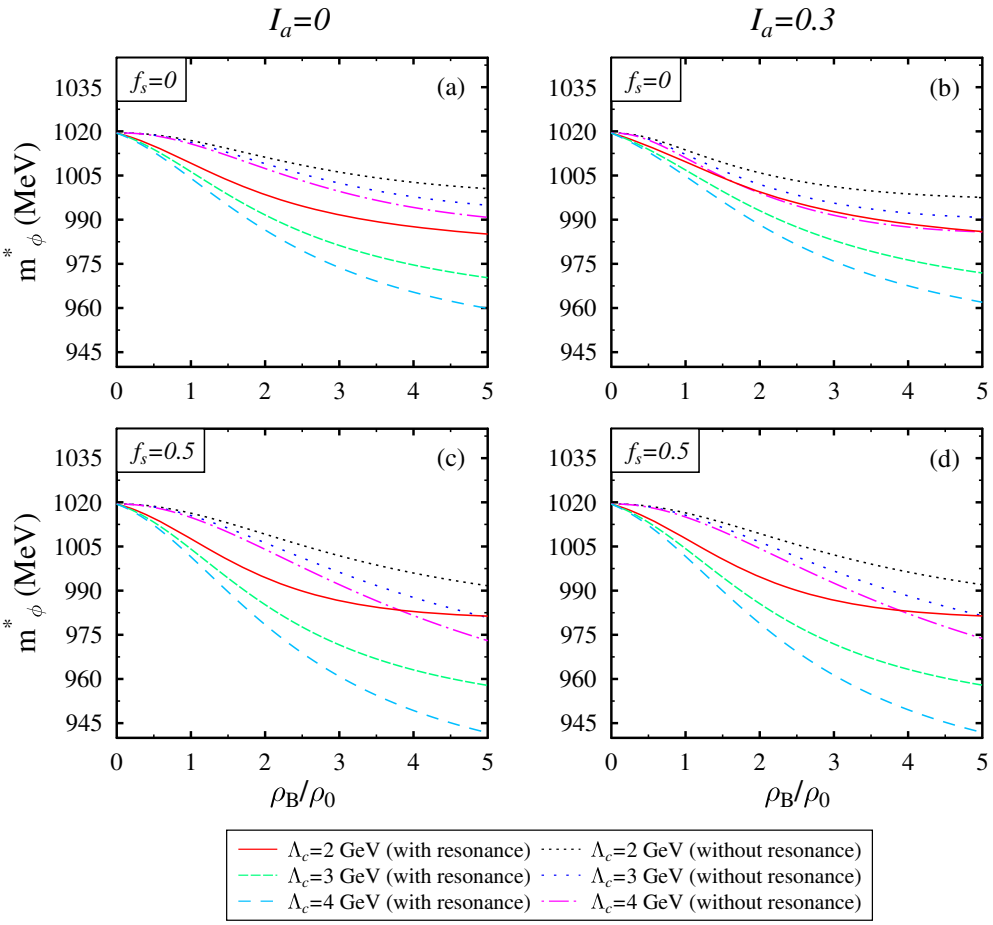


FIG. 5. The comparison of m^*_ϕ in both resonance and non-resonance matter is presented as a function of baryon density ratio ρ_B/ρ_0, considering various values of Λ_c, I_a, and f_s at temperature $T = 100$ MeV. The results corresponding to isospin asymmetry parameters $I_a = 0$ and 0.3 are displayed for the strangeness fractions $f_s = 0$ in subplots (a) and (b), and $f_s = 0.5$ in subplots (c) and (d).

nuclear saturation density, ρ_0, average kaons (antikaons) mass shift of 22 (−44.5) and 15 (−78.3) MeV leads to change in the ϕ meson mass by −5 and −13 MeV, respectively. At $f_s = 0.5$, these mass shift values for K ($\bar{K}$) change to −11.5 (−16.7) and −17.7 (−58) MeV inducing shift of −6.3 and −15.7 MeV in m^*_ϕ. For a given baryon density ρ_B, mass m^*_ϕ is observed to decrease with an increase of Λ_c, for all different environments. These findings align with results from previous studies, where in-medium ϕ meson masses were calculated in nuclear medium [88,89] and hyperonic medium [48]. The studies in Refs. [88,48] observed that the vacuum ϕ meson mass (1020 MeV) falls to 994.9 and 1017.4 MeV, respectively, in nuclear medium at $\Lambda_c = 3$ GeV, $\rho_B = \rho_0$, and $T = 0$ MeV. The larger shift in m^*_ϕ observed in Ref. [88] can be attributed to the omission of the difference

TABLE II. The in-medium values of m^*_ϕ at different fixed values of Λ_c, ρ_B, I_a, f_s, and T.

		T = 0 MeV				T = 100 MeV				T = 150 MeV			
		$I_a = 0$		$I_a = 0.3$		$I_a = 0$		$I_a = 0.3$		$I_a = 0$		$I_a = 0.3$	
m^*_ϕ (MeV)	f_s	ρ_0	$4\rho_0$	ρ_0	$4\rho_0$	ρ_0	$4\rho_0$	ρ_0	$4\rho_0$	ρ_0	$4\rho_0$	ρ_0	$4\rho_0$
$\Lambda_c = 2$ GeV	0	1015.7	999.1	1015.8	999.9	1009.2	987.6	1009.6	988.6	1002.9	983.8	1002.9	983.8
	0.5	1014.8	991.1	1014.9	992.0	1007.6	982.9	1007.7	983.0	999.4	981.1	999.0	981.1
$\Lambda_c = 3$ GeV	0	1014.8	992.6	1014.9	993.8	1006.3	974.6	1006.9	976.3	997.8	966.8	997.7	966.8
	0.5	1013.5	979.7	1013.7	981.2	1004.1	963.1	1004.3	963.3	992.8	954.3	992.1	953.6
$\Lambda_c = 4$ GeV	0	1014.1	987.8	1014.2	989.3	1004.1	965.4	1004.8	967.6	993.9	955.0	993.8	954.9
	0.5	1012.6	971.4	1012.7	973.3	1001.5	949.3	1001.6	949.5	987.7	936.2	986.9	935.1

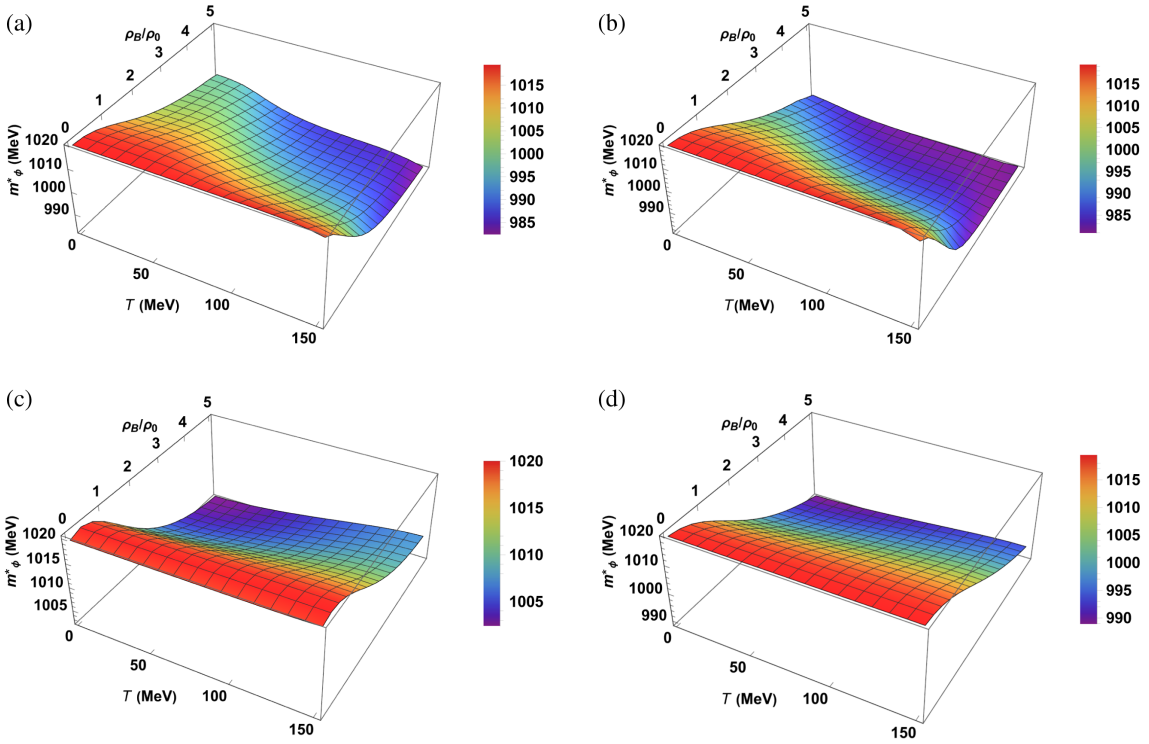


FIG. 6. The three-dimensional representation of effective masses of ϕ meson is plotted as a function of baryon density ratio ρ_B/ρ_0 and temperature T for isospin asymmetry $I_a = 0.3$ and cutoff parameter $\Lambda_c = 2$ GeV. The left panel corresponds to $f_s = 0$, with (a) including both nucleons and Δ baryons, while (c) considers only nucleons. The right panel is for $f_s = 0.5$, where (b) incorporates all octet and decuplet baryons and (d) involves octet baryons only.

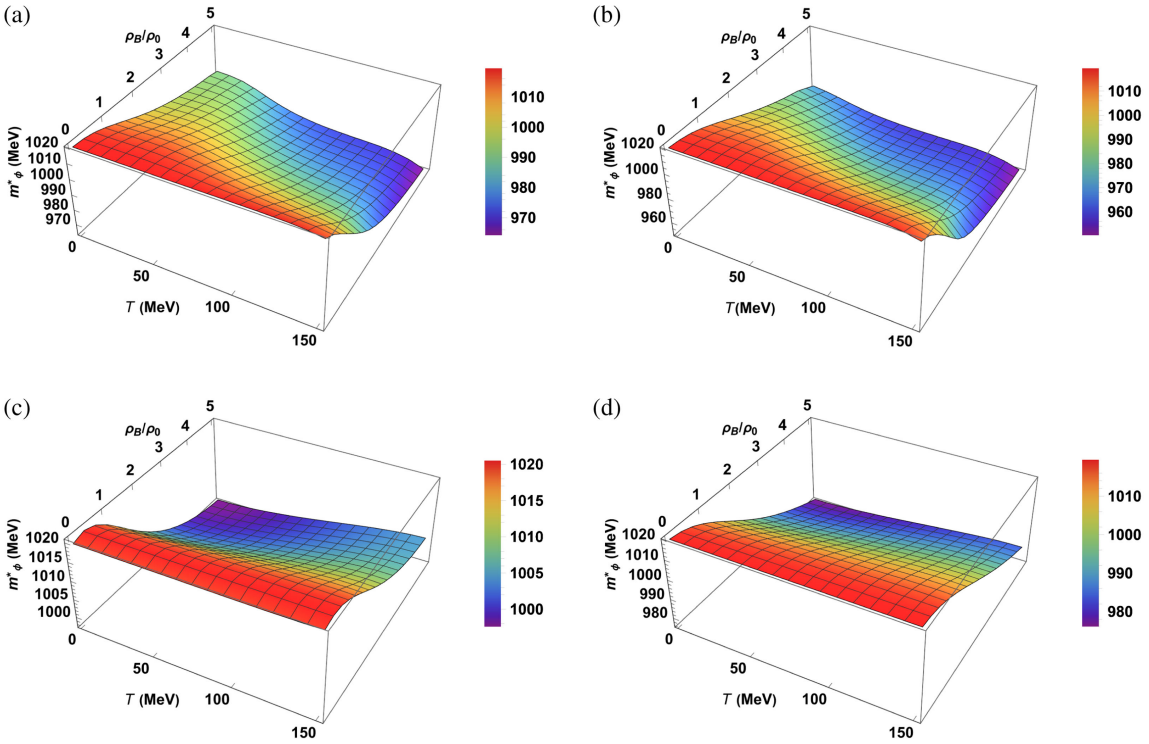


FIG. 7. The three-dimensional representation of effective masses of ϕ meson is plotted as a function of baryon density ratio ρ_B/ρ_0 and temperature T for isospin asymmetry $I_a = 0.3$ and cutoff parameter $\Lambda_c = 3$ GeV. The left panel corresponds to $f_s = 0$, with (a) includes both nucleons and Δ baryons, while (c) considers only nucleons. The right panel is for $f_s = 0.5$, where (b) incorporates all octet and decuplet baryons and (d) involves octet baryons only.

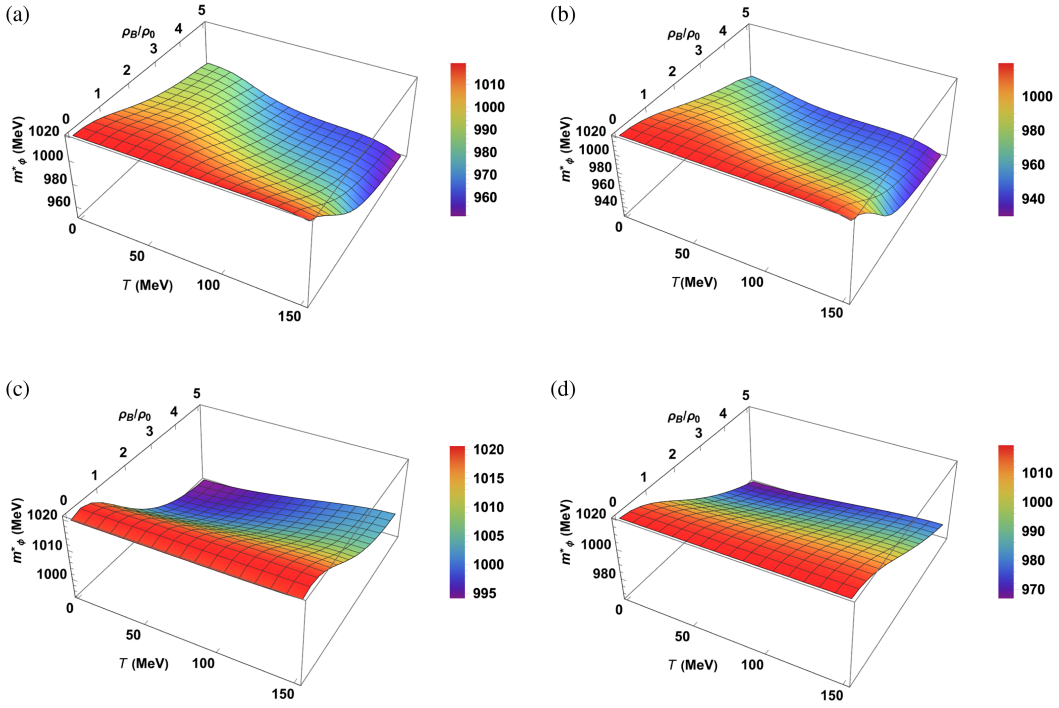


FIG. 8. The three-dimensional representation of effective masses of ϕ meson is plotted as a function of baryon density ratio ρ_B/ρ_0 and temperature T for isospin asymmetry $I_a = 0.3$ and cutoff parameter $\Lambda_c = 4$ GeV. The left panel corresponds to $f_s = 0$, with (a) includes both nucleons and Δ baryons, while (c) considers only nucleons. The right panel is for $f_s = 0.5$, where (b) incorporates all octet and decuplet baryons and (d) involves octet baryons only.

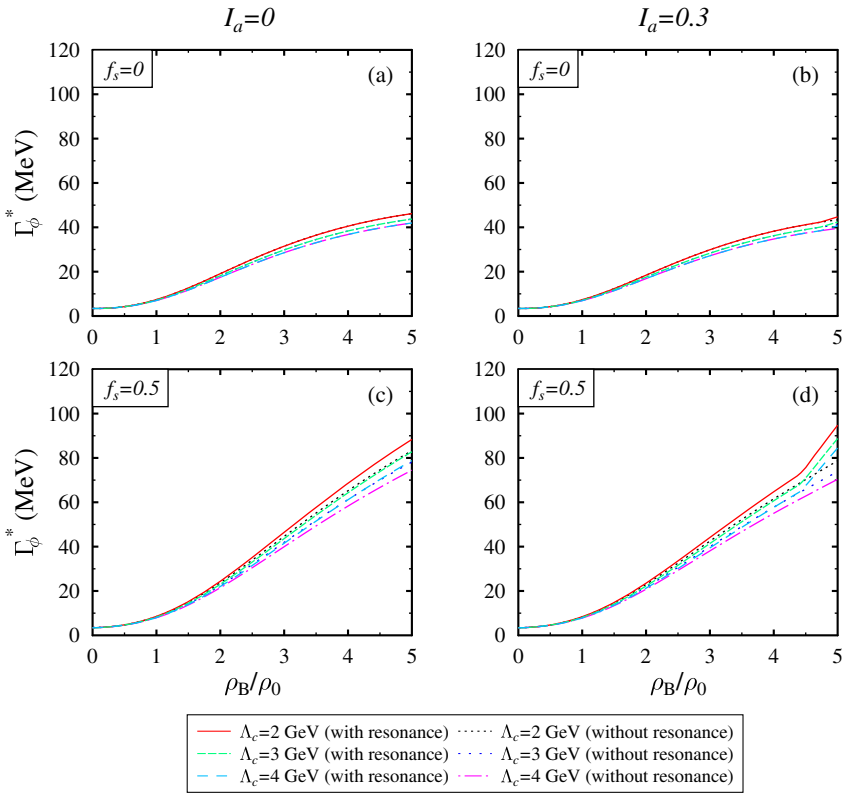


FIG. 9. The in-medium decay width Γ^*_ϕ of ϕ meson is plotted for dense resonance matter with respect to baryon density ratio ρ_B/ρ_0 for various values of Λ_c, I_a, and f_s at temperature $T = 0$ MeV. Each subplot also compares the cases in which decuplet baryons are not taken into account within the medium. For each value of the isospin asymmetry parameter ($I_a = 0$ and 0.3), the corresponding results are presented for $f_s = 0$ in subplots (a) and (b), and for $f_s = 0.5$ in subplots (c) and (d).

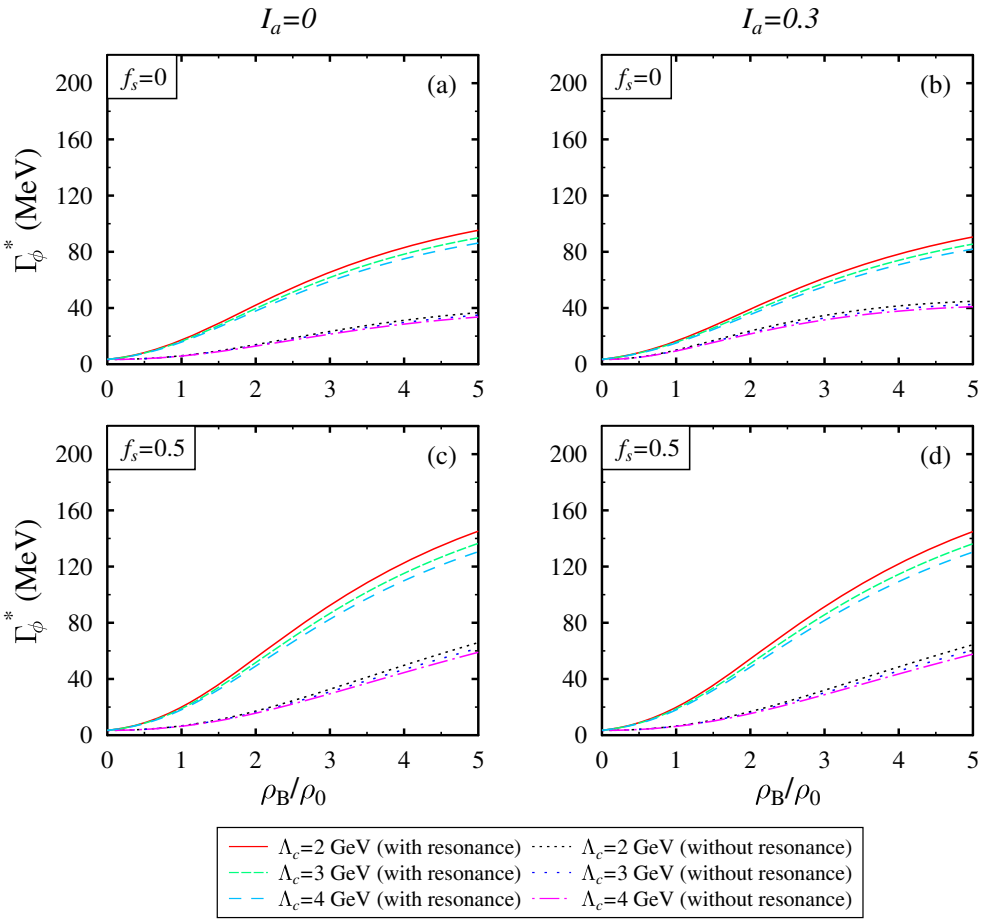


FIG. 10. The in-medium decay width Γ_ϕ^* of the ϕ meson is plotted for dense resonance matter with respect to baryon density ratio ρ_B/ρ_0 for various values of Λ_c, I_a, and f_s at temperature $T = 100$ MeV. These findings are compared in each subplot with the situation in which only spin-1/2 baryons are considered. For each value of the isospin asymmetry parameter ($I_a = 0$ and 0.3), the corresponding results are presented for $f_s = 0$ in subplots (a) and (b), and for $f_s = 0.5$ in subplots (c) and (d).

between m_K^* and $m_{\bar{K}}^*$ in their calculations, reporting a mass shift of roughly -64 MeV for both K and $\bar{K}$ at ρ_0. At $T = 0$ MeV, in Refs. [98,99,142], nearly 1% mass shift for ϕ mesons was observed in the QCD sum rules calculations.

In Figs. 6–8, we show the 3D plots for visualization of density and temperature dependence of the in-medium ϕ meson masses, at $\Lambda_c = 2$, 3, and 4 GeV, respectively. Figures 6(a) and 6(c) illustrate an isospin asymmetric nonstrange medium, with (a) including n, p and $\Delta^{++,+,0,-}$ baryons, while (c) includes only nucleons. Calculations considering only nucleons exhibit a significant decrease in m_ϕ^* as temperature drops, whereas incorporating Δ baryons, the opposite trend of ϕ meson mass is observed. The subplots (b) and (d) of Fig. 6 represent

TABLE III. The in-medium values of Γ_ϕ^* at different fixed values of Λ_c, ρ_B, I_a, f_s, and T.

		T = 0 MeV				T = 100 MeV				T = 150 MeV			
		$I_a = 0$		$I_a = 0.3$		$I_a = 0$		$I_a = 0.3$		$I_a = 0$		$I_a = 0.3$	
Γ_ϕ^* (MeV)	f_s	ρ_0	$4\rho_0$	ρ_0	$4\rho_0$	ρ_0	$4\rho_0$	ρ_0	$4\rho_0$	ρ_0	$4\rho_0$	ρ_0	$4\rho_0$
$\Lambda_c = 2$ GeV	0	7.4	40.5	7.3	38.2	17.2	83.0	16.4	78.3	30.1	107.1	30.2	107.5
	0.5	8.5	68.6	8.4	64.7	20.0	122.6	19.8	121.9	39.0	163.8	40.3	167.9
$\Lambda_c = 3$ GeV	0	7.2	38.3	7.1	36.2	16.4	78.3	15.7	73.9	28.4	100.9	28.5	101.2
	0.5	8.2	64.3	8.1	60.7	18.9	115.2	18.8	114.5	36.7	154.1	37.9	158.1
$\Lambda_c = 4$ GeV	0	7.0	36.8	6.9	34.7	15.7	75.0	15.1	70.8	27.2	96.6	27.3	96.9
	0.5	8.0	61.2	7.9	57.7	18.1	110.0	18.0	109.3	34.9	147.6	36.1	151.4

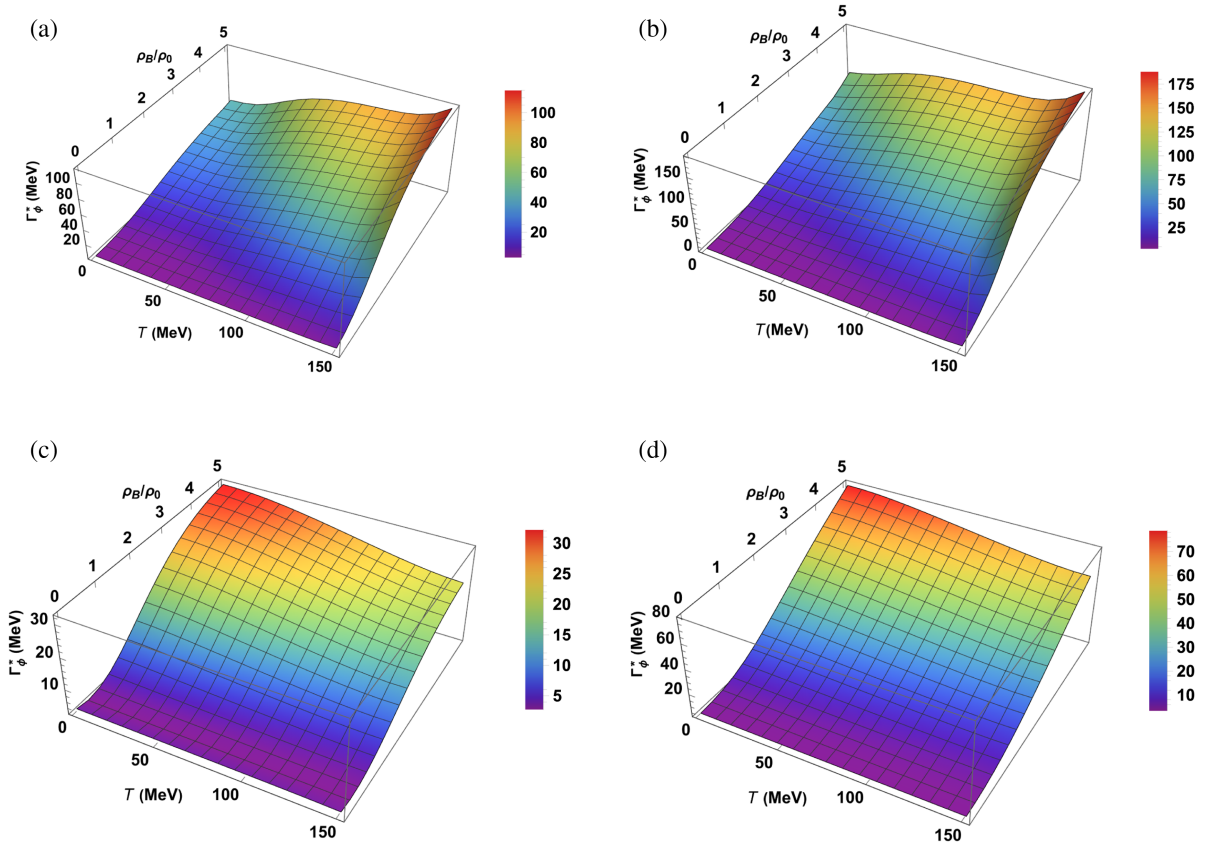


FIG. 11. The 3D representation of the in-medium decay width of ϕ meson is plotted as a function of baryon density ratio ρ_B/ρ_0 and temperature T for an isospin asymmetric medium ($I_a = 0.3$) with the cutoff parameter $\Lambda_c = 2$ GeV. The subplots (a) and (c) correspond to $f_s = 0$, with (a) incorporating both nucleons and Δ baryons, while (c) involves only nucleons. The subplots (b) and (d) are for $f_s = 0.5$, where (b) includes all octet and decuplet baryons and (d) involves octet baryons only.

$f_s = 0.5$ and $I_a = 0.3$, with (b) involving all octet and decuplet baryons and (d) including octet baryons only. Consideration of all spin-3/2 resonance baryons along with the spin-1/2 octet in Fig. 6(b) produces a trend comparable to that of Fig. 6(a), but a more noticeable modification in m^*_ϕ has been observed in Fig. 6(b) as a function of T and the ρ_B/ρ_0 ratio. As shown in Figs. 7 and 8, an increase in the cutoff mass value results in a more significant decrease in m^*_ϕ.

C. In-medium decay width of ϕ meson in resonance matter

This subsection addresses how resonance production within the medium influences the probability of ϕ meson decay. As discussed earlier in Sec. II C, the decay width of ϕ meson is derived from the imaginary part of the self-energy $\mathrm{Im}\,\Pi^*_\phi$. Figures 9 and 10 show the behavior of the in-medium decay width of the ϕ meson as a function of baryonic density in isospin-dependent resonance medium for the different values of $\Lambda_c = 2, 3, 4$ GeV, at temperatures $T = 0$ and 100 MeV. Table III presents the medium-modified values of decay width of ϕ meson Γ^*_ϕ within the resonance medium for various values of Λ_c, ρ_B, I_a, f_s, and T. We have noticed that raising the baryonic density leads to an increase in Γ^*_ϕ for all scenarios involving different values of f_s, I_a, Λ_c, and T. In Figs. 9(a) and 9(b), the medium modification of Γ^*_ϕ as a function of ρ_B/ρ_0, with and without Δ baryon resonances, remains the same. Further inclusion of strange baryons gives a more appreciable increase in Γ^*_ϕ as illustrated in Figs. 9(c) and 9(d). Notably, the rate of increase in Γ^*_ϕ is more substantial in presence of resonance baryons, as the cutoff mass parameter increases, for all values of ρ_B. In Fig. 10, the decay width of ϕ meson at finite temperature exhibits a pattern similar to that observed at zero temperature. However, there is a more pronounced increase in Γ^*_ϕ with respect to baryonic density at higher temperatures.

We portray a 3D representation of the decay width of ϕ mesons as a function of baryon density ratio ρ_B/ρ_0 and temperature T, at fixed values of $\Lambda_c = 2$, 3, and 4 GeV in Figs. 11–13, respectively. Within a pure nuclear medium at low temperature, there is a rise in Γ^*_ϕ with increasing density, while at a higher temperature, the rate of increase becomes slower at $\Lambda_c = 2$ GeV as exhibited in Fig. 11(c).

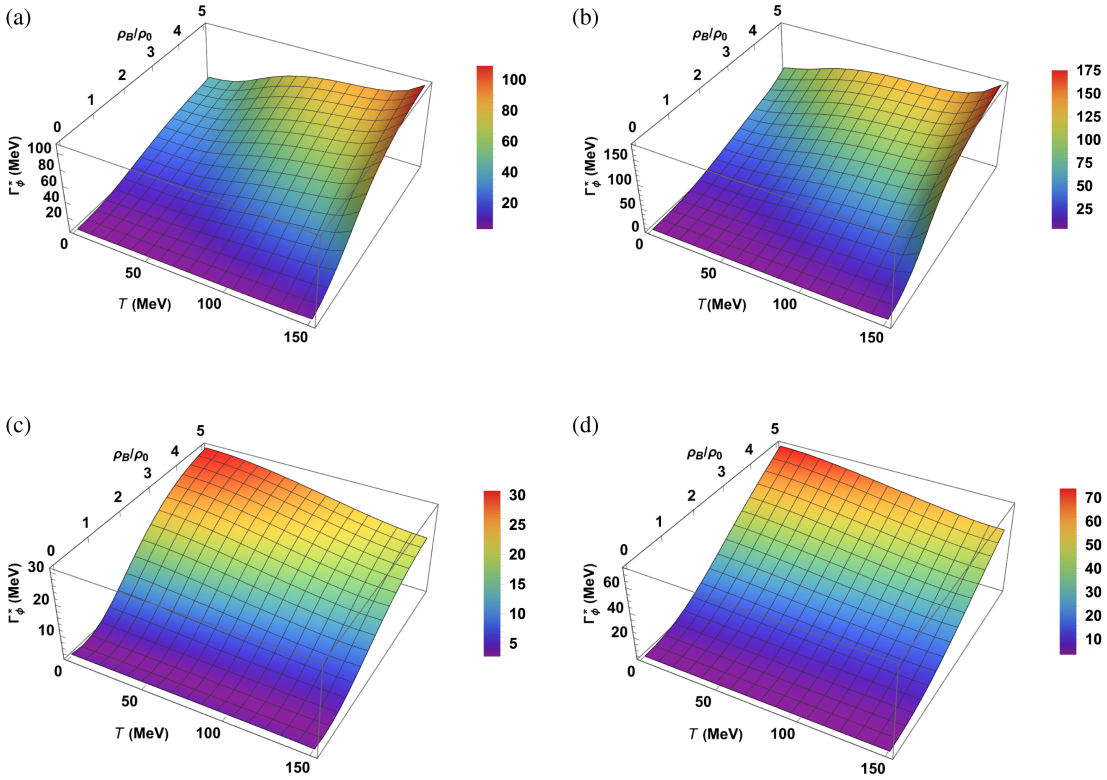


FIG. 12. The 3D representation of the in-medium decay width of ϕ meson is plotted as a function of baryon density ratio ρ_B/ρ_0 and temperature T for an isospin asymmetric medium ($I_a = 0.3$) with the cutoff parameter $\Lambda_c = 3$ GeV. The subplots (a) and (c) correspond to $f_s = 0$, with (a) incorporating both nucleons and Δ baryons while (c) involves only nucleons. The subplots (b) and (d) are for $f_s = 0.5$, where (b) includes all octet and decuplet baryons and (d) involves octet baryons only.

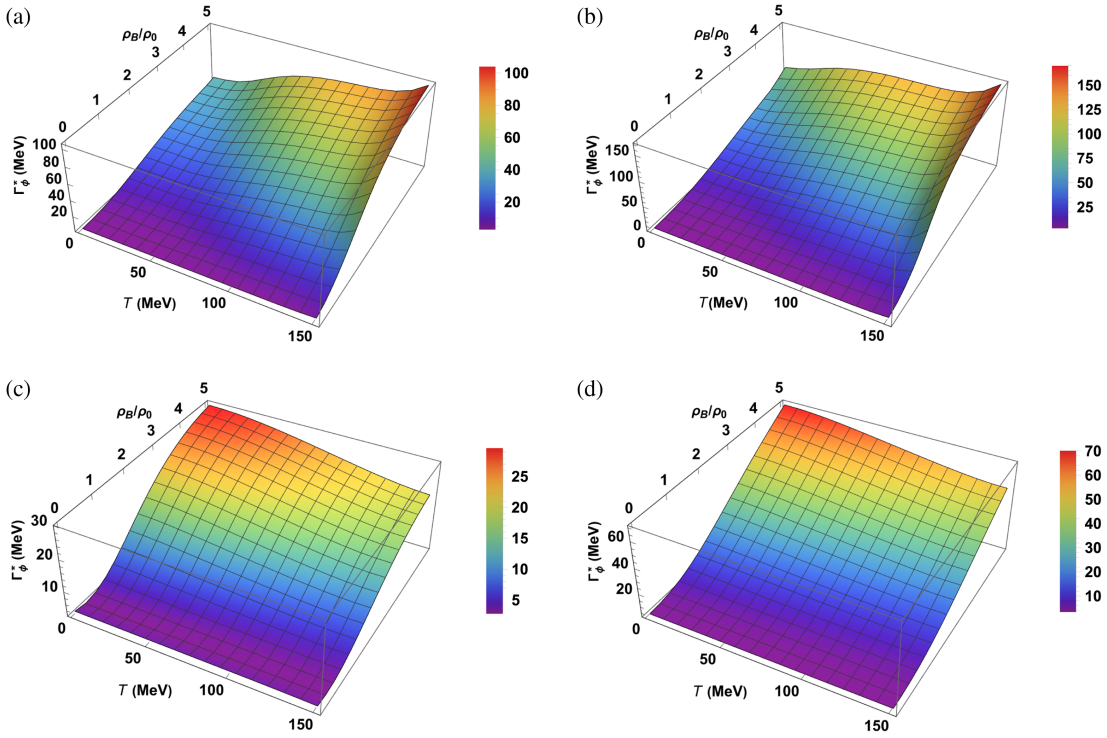


FIG. 13. The 3D representation of the in-medium decay width of ϕ meson is plotted as a function of baryon density ratio ρ_B/ρ_0 and temperature T for an isospin asymmetric medium ($I_a = 0.3$) with the cutoff parameter $\Lambda_c = 4$ GeV. The subplots (a) and (c) correspond to $f_s = 0$, with (a) incorporating both nucleons and Δ baryons while (c) involves only nucleons. The subplots (b) and (d) are for $f_s = 0.5$, where (b) includes all octet and decuplet baryons and (d) involves octet baryons only.

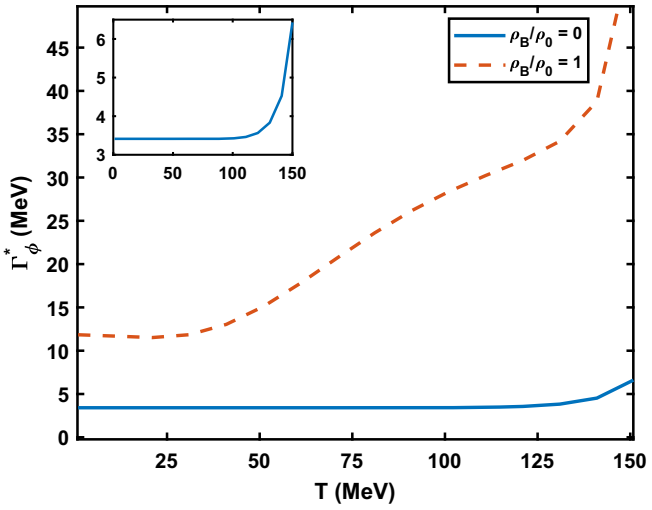


FIG. 14. Temperature dependence of ϕ meson decay width in resonance matter at $\rho_B = 0$ and ρ_0. For finite ρ_B, isospin asymmetry parameter I_a is fixed at 0.3.

When we involve Δ baryons within the nuclear medium, the rate of increase becomes faster at higher temperatures as shown in Fig. 11(a). Furthermore, in Fig. 11(d), we observed a comparable trend of Γ^*_ϕ as in Fig. 11(c) because both figures consider spin-1/2 baryons only. Figure 11(b) involves all spin-1/2 and $-3/2$ baryons, and the rate of increase in Γ^*_ϕ becomes notably more rapid as temperature of the medium increases. Noticeably, at even zero baryon density, our results show a growing behavior of the ϕ meson decay width as a function of temperature within the resonance medium as depicted in Fig. 14. As shown in figure, this behavior becomes more pronounced at finite baryon density, where the medium effects become stronger.

Figures 12 and 13 show that as Λ_c increases at given ρ_B/ρ_0 the rate of increase in Γ^*_ϕ exhibits a decreasing trend in both the resonance and nonresonance cases, as can be seen in Table IV, where the comparison of Γ^*_ϕ of the nuclear and resonance matters is listed at $T = 0$ and 100 MeV for $I_a = 0.3$. The findings from the present study align with the outcomes reported in Ref. [88], indicating a reduction in decay width when Λ_c is altered from 2 to 4 GeV. Reference [143] examines the self-energy of ϕ for a symmetric nuclear environment. This analysis involves incorporating the self-energies of S and P waves. The self-consistent coupled channel calculation, based on effective chiral Lagrangians was employed to determine the S-wave $\bar{K}$ self-energy. The P-wave component is influenced by hyperon-hole excitation couplings. The results indicate a ϕ meson mass shift of approximately 8 MeV and a width of about 30 MeV in the nuclear medium at nuclear saturation density.

TABLE IV. The values of Γ^*_ϕ (MeV) for different Λ_c in isospin asymmetric nuclear and resonance matter at $T = 0$ MeV and $T = 100$ MeV at nuclear saturation density, $\rho_B = \rho_0$.

	Nuclear matter		Resonance matter	
Γ^*_ϕ (MeV)	$T = 0$ MeV	$T = 100$ MeV	$T = 0$ MeV	$T = 100$ MeV
$\Lambda_c = 2$ GeV	7.30	10	8.4	19.8
$\Lambda_c = 3$ GeV	7.09	9.7	8.1	18.8
$\Lambda_c = 4$ GeV	6.93	9.4	7.9	18.0

IV. CONCLUSIONS

To conclude, we examine the in-medium properties of the ϕ meson in isospin asymmetric resonance medium through the medium modifications of K and $\bar{K}$ meson masses. Employing a mean-field approximation within the chiral SU(3) framework, we compute the medium-modified properties of baryons by exchange of scalar fields σ, ζ, and δ and vector fields ω, ρ, and ϕ. Vector and scalar densities of baryons and in-medium scalar meson fields σ, and ζ, and δ serve as input to analyze the behavior of effective masses of K and $\bar{K}$ mesons in a dense resonance environment. The medium-modified masses of kaons and antikaons are further utilized to determine the ϕ meson masses and decay width in isospin asymmetric resonance matter. Considering the presence of resonance baryons, we observe attractive interactions (negative mass shift) for kaon and antikaon masses at higher baryon density and temperature of the medium. Because of this, the decay width of the ϕ meson is observed to increase in presence of resonance baryons. At temperature $T = 100$ MeV, the effective masses of kaons and antikaons are observed to decrease by 3.6% and 11.8%, respectively. This results in a 1.56% reduction in the mass of the ϕ meson within an isospin asymmetric resonance medium at nuclear saturation density.

As previously mentioned, the in-medium properties of vector mesons are utilized as input in various transport models to simulate and predict the results of different experiments [77,101,144,145]. The future experiment E16 at J-PARC examines dielectron spectra to investigate how vector mesons spectral properties change within the medium, which indicates a partial restoration of broken symmetry. Furthermore, this experiment will measure the ϕ meson spectrum at both zero and finite momentum [146]. In practical applications, the decay width serves as a valuable tool for evaluating ϕ meson creation in $p - N$ collisions. The production, absorption, and momentum spectrum of ϕ meson within the hadronic environment are expected to be addressed through the findings of experiments like CBM and PANDA at FAIR [16,19,147].

ACKNOWLEDGMENTS

The authors sincerely acknowledge the support for this work from the Ministry of Science and Human Resources (MHRD), Government of India, through an Institute fellowship under the National Institute of Technology

Jalandhar. A. K. sincerely acknowledges Anusandhan National Research Foundation (ANRF), Government of India, for funding of the research project under the Science and Engineering Research Board-Core Research Grant (SERB-CRG) scheme (File No. CRG/2023/000557).

DATA AVAILABILITY

The data that support the findings of this article are not publicly available. The data are available from the authors upon reasonable request.

[1] S. Leupold, V. Metag, and U. Mosel, Int. J. Mod. Phys. E **19**, 147 (2010).
[2] R. S. Hayano and T. Hatsuda, Rev. Mod. Phys. **82**, 2949 (2010).
[3] T. Maruyama, S. Chiba, H.-J. Schulze, and T. Tatsumi, Phys. Lett. B **659**, 192 (2008).
[4] P. Wang *et al.*, Phys. Rev. C **75**, 045202 (2007).
[5] L. Tolos and L. Fabbietti, Prog. Part. Nucl. Phys. **112**, 103770 (2020).
[6] I. Pushkina, P. d. Forcrand, M. Garcia Perez, S. Kim, H. Matsufuru, A. Nakamura, I.-O. Stamatescu, T. Takaishi, and T. Umeda, Phys. Lett. B **609**, 265 (2005).
[7] J. Rafelski and J. Letessier, Phys. Rev. Lett. **85**, 4695 (2000).
[8] A. G. Knospe, EPJ Web Conf. **171**, 09001 (2018).
[9] M. Harrison, T. Ludlam, and S. Ozaki, Nucl. Instrum. Methods Phys. Res., Sect. A **499**, 235 (2003).
[10] B. Friman, C. Höhne, J. Knoll, S. Leupold, J. Randrup, R. Rapp, and P. Senger, Lect. Notes Phys. **814**, 1 (2011).
[11] L. Kumar *et al.*, Nucl. Phys. **A904**, 256c (2013).
[12] G. Odyniec, J. Phys. G **37**, 094028 (2010).
[13] L. Evans, New J. Phys. **9**, 335 (2007).
[14] P. Di Nezza *et al.*, Proc. Sci. SPIN2023 (**2024**) 036.
[15] K. Agarwal, Phys. Scr. **98**, 034006 (2023).
[16] P. Senger, Central Eur. J. Phys. **10**, 1289 (2012).
[17] T. Nilsson, Phys. Scr. T **166**, 014070 (2015).
[18] A. Herlert, EPJ Web Conf. **71**, 00064 (2014).
[19] R. Rapp, D. Blaschke, and P. Crochet, Prog. Part. Nucl. Phys. **65**, 209 (2010).
[20] S. Sawada, Nucl. Phys. **A782**, 434 (2007).
[21] H. Hotchi *et al.*, Phys. Rev. Accel. Beams **20**, 060402 (2017).
[22] V. D. Kekelidze, V. A. Matveev, I. N. Meshkov, A. S. Sorin, and G. V. Trubnikov, Phys. Part. Nucl. **48**, 727 (2017).
[23] V. D. Kekelidze *et al.*, Nucl. Phys. **A967**, 884 (2017).
[24] A. Milov, Eur. Phys. J. C **61**, 721 (2009).
[25] K. G. Wilson, Phys. Rev. D **10**, 2445 (1974).
[26] A. Alexandru, G. Başar, P. F. Bedaque, and N. C. Warrington, Rev. Mod. Phys. **94**, 015006 (2022).
[27] J. Bloch and T. Wettig, J. High Energy Phys. 03 (2009) 100.
[28] K. Fukushima and Y. Hidaka, Phys. Rev. D **75**, 036002 (2007).
[29] S. Muroya, A. Nakamura, C. Nonaka, and T. Takaishi, Prog. Theor. Phys. **110**, 615 (2003).
[30] T. Takaishi, Prog. Theor. Phys. Suppl. **153**, 277 (2004).
[31] K. Tsushima *et al.*, Phys. Rev. C **59**, 2824 (1999).
[32] K. Saito and A. W. Thomas, Phys. Lett. B **327**, 9 (1994).
[33] K. Tsushima, K. Saito, J. Haidenbauer, and A. W. Thomas, Nucl. Phys. **A630**, 691 (1998).
[34] G. Cao, Eur. Phys. J. A **57**, 264 (2021).
[35] A. Bochkarev and J. I. Kapusta, Phys. Rev. D **54**, 4066 (1996).
[36] P. Huovinen and P. Petreczky, Nucl. Phys. **A837**, 26 (2010).
[37] S. R. Wadia, Phys. Rev. D **24**, 970 (1981).
[38] A. Pich, Rep. Prog. Phys. **58**, 563 (1995).
[39] S. Scherer, Adv. Nucl. Phys. **27**, 277 (2003).
[40] T. Waas, M. Rho, and W. Weise, Nucl. Phys. **A617**, 449 (1997).
[41] T. Hatsuda, and S. H. Lee, Phys. Rev. C **46**, R34 (1992).
[42] A. Kumar and A. Mishra, Eur. Phys. J. A **47**, 164 (2011).
[43] Z. Y. Zhang, Y. W. Yu, P. N. Shen, L. R. Dai, A. Faessler, and U. Straub, Nucl. Phys. **A625**, 59 (1997).
[44] P. Wang, D. B. Leinweber, A. W. Thomas, and A. G. Williams, Nucl. Phys. **A744**, 273 (2004).
[45] P. Papazoglou *et al.*, Phys. Rev. C **59**, 411 (1999).
[46] A. Mishra, A. Kumar, S. Sanyal, V. Dexheimer, and S. Schramm, Eur. Phys. J. A **45**, 169 (2010).
[47] V. Dexheimer and S. Schramm, Astrophys. J. **683**, 943 (2008).
[48] R. Kumar and A. Kumar, Phys. Rev. C **102**, 045206 (2020).
[49] N. Chahal *et al.*, Eur. Phys. J. C **84**, 1028 (2024).
[50] D. Zschiesche *et al.*, Phys. Rev. C **70**, 045202 (2004).
[51] N. Cruz-Camacho, R. Kumar, M. Reinke Pelicer, J. Peterson, T. A. Manning, R. Haas, V. Dexheimer, and J. Noronha-Hostler, Phys. Rev. D **111**, 094030 (2025).
[52] M. Kaur and A. Kumar, Phys. Rev. D **110**, 114054 (2024).
[53] B.-J. Schaefer, J. M. Pawlowski, and J. Wambach, Phys. Rev. D **76**, 074023 (2007).
[54] T. K. Herbst, J. M. Pawlowski, and B.-J. Schaefer, Phys. Lett. B **696**, 58 (2011).
[55] R. Stiele, E. S. Fraga, and J. Schaffner-Bielich, Phys. Lett. B **729**, 72 (2014).
[56] A. Ramos and E. Oset, Nucl. Phys. **A671**, 481 (2000).
[57] J. Schaffner-Bielich, V. Koch, and M. Effenberger, Nucl. Phys. **A669**, 153 (2000).
[58] M. Lutz, Phys. Lett. B **426**, 12 (1998).
[59] L. Tolós, J. Schaffner-Bielich, and A. Mishra, Phys. Rev. C **70**, 025203 (2004).
[60] L. Tolós, J. Schaffner-Bielich, and H. Stöcker, Phys. Lett. B **635**, 85 (2006).
[61] L. Tolós, A. Ramos, and T. Mizutani, Phys. Rev. C **77**, 015207 (2008).
[62] Y.-F. Wang, EPJ Web Conf. **291**, 02004 (2024).

[63] W.-Y. Liu and H.-X. Chen, Eur. Phys. J. C **85**, 636 (2025).
[64] D. J. Wilson, C. E. Thomas, J. J. Dudek, and R. G. Edwards, Phys. Rev. Lett. **132**, 241901 (2024).
[65] J. Rozynek and G. Wilk, J. Phys. G **36**, 125108 (2009).
[66] A. Adel and T. Alharbi, Eur. Phys. J. A **53**, 1 (2017).
[67] G. S. Bali, F. Bruckmann, G. Endrődi, Z. Fodor, S. D. Katz, S. Krieg, A. Schäfer, and K. K. Szabó, J. High Energy Phys. 02 (2012) 044.
[68] G. S. Bali *et al.*, Proc. Sci. ConfinementX2012 (**2012**) 197.
[69] J. Peterson, P. Costa, R. Kumar, V. Dexheimer, R. Negreiros, and C. Providência, Phys. Rev. D **108**, 063011 (2023).
[70] A. Bhattacharyya, R. Ray, S. Samanta, and S. Sur, Phys. Rev. C **91**, 041901 (2015).
[71] N. Magdy, M. Csanád, and R. A. Lacey, J. Phys. G **44**, 025101 (2017).
[72] J. Braun, B. Klein, and B.-J. Schaefer, Phys. Lett. B **713**, 216 (2012).
[73] M. Ruggieri and G. X. Peng, Phys. Rev. D **93**, 094021 (2016).
[74] M. Ruggieri, Z. Y. Lu, and G. X. Peng, Phys. Rev. D **94**, 116003 (2016).
[75] P. Senger, Nucl. Phys. **A835**, 102 (2010).
[76] G.-C. Yong, Phys. Rev. D **108**, L091507 (2023).
[77] T. Song, J. Aichelin, and E. Bratkovskaya, Phys. Rev. C **106**, 024903 (2022).
[78] S. Okubo, Phys. Lett. **5**, 165 (1963).
[79] J. Iizuka, Prog. Theor. Phys. Suppl. **37**, 21 (1966).
[80] H. J. Lipkin, Nucl. Phys. **B244**, 147 (1984).
[81] M. Asakawa and C. Ko, Nucl. Phys. **A572**, 732 (1994).
[82] T. Hatsuda, H. Shiomi, and H. Kuwabara, Prog. Theor. Phys. **95**, 1009 (1996).
[83] J.-P. Blaizot and R. M. Galain, Phys. Lett. B **271**, 32 (1991).
[84] H. Kuwabara and T. Hatsuda, Prog. Theor. Phys. **94**, 1163 (1995).
[85] E. Oset, M. J. Vicente Vacas, H. Toki, and A. Ramos, Phys. Lett. B **508**, 237 (2001).
[86] A. Bhattacharyya, S. K. Ghosh, S. C. Phatak, and S. Raha, Phys. Rev. C **55**, 1463 (1997).
[87] F. Klingl, N. Kaiser, and W. Weise, Nucl. Phys. **A624**, 527 (1997).
[88] J. J. Cobos-Martínez, K. Tsushima, G. Krein, and A. W. Thomas, Phys. Lett. B **771**, 113 (2017).
[89] J. J. Cobos-Martínez *et al.*, Phys. Rev. C **96**, 035201 (2017).
[90] R. Muto *et al.*, Phys. Rev. Lett. **98**, 042501 (2007).
[91] T. Mibe *et al.*, Phys. Rev. C **76**, 052202 (2007).
[92] X. Qian, W. Chen *et al.*, Phys. Lett. B **680**, 417 (2009).
[93] T. Ishikawa *et al.*, Phys. Lett. B **608**, 215 (2005).
[94] H. Sako *et al.*, J. Subatomic Part. Cosmol. **1–2**, 100012 (2024).
[95] K. Aoki *et al.*, J. Subatomic Part. Cosmol. **3**, 100019 (2025).
[96] W. T. Chiang, B. Saghai, F. Tabakin, and T.-S. H. Lee, Phys. Rev. C **69**, 065208 (2004).
[97] M. Lutz, Phys. Lett. B **426**, 12 (1998).
[98] F. Klingl, T. Waas, and W. Weise, Phys. Lett. B **431**, 254 (1998).
[99] P. Gubler and K. Ohtani, Phys. Rev. D **90**, 094002 (2014).
[100] W. S. Chung, G.-Q. Li, and C. M. Ko, Nucl. Phys. **A625**, 347 (1997).
[101] S. Pal, C. M. Ko, and Z.-w. Lin, Nucl. Phys. **A707**, 525 (2002).
[102] E. Y. Paryev, Nucl. Phys. **A1032**, 122624 (2023).
[103] A. Kumar and A. Mishra, Chin. Phys. C **49**, 074106 (2025).
[104] A. Mondal and A. Mishra, Phys. Rev. D **111**, 094037 (2025).
[105] Z.-H. Tu and S.-G. Zhou, Astrophys. J. **925**, 16 (2022).
[106] C. Wu and W. Guo, Eur. Phys. J. Plus **140**, 193 (2025).
[107] J. Song, J. Phys. Conf. Ser. **1602**, 012008 (2020).
[108] J. Lömker, Proc. Sci. EPS-HEP2023 (**2024**) 216.
[109] A. Rosano, Proc. Sci. ICHEP2022 (**2022**) 1066.
[110] S. Kiselev, Phys. At. Nucl. **85**, 965 (2022).
[111] P. F. Bedaque, Phys. Lett. B **387**, 1 (1996).
[112] J. M. Torres-Rincon, B. Sintes, and J. Aichelin, Phys. Rev. C **91**, 065206 (2015).
[113] Y.-J. Xu, Y.-L. Liu, and M.-Q. Huang, Commun. Theor. Phys. **63**, 209 (2015).
[114] K. Azizi and G. Bozkır, Eur. Phys. J. C **76**, 521 (2016).
[115] K. Azizi, N. Er, and H. Sundu, Phys. Rev. D **94**, 114002 (2016).
[116] S. M. Ouellette and R. Seki, Phys. Lett. B **404**, 108 (1997).
[117] A. Kumar, S. Dutt, and H. Dahiya, Eur. Phys. J. A **60**, 4 (2024).
[118] C. Y. Ryu, C. H. Hyun, T.-S. Park, and S. W. Hong, Phys. Lett. B **674**, 122 (2009).
[119] H. Singh, A. Kumar, and H. Dahiya, Eur. Phys. J. Plus **134**, 128 (2019).
[120] H. Singh, A. Kumar, and H. Dahiya, Eur. Phys. J. Plus **135**, 422 (2020).
[121] D. Zschiesche, P. Papazoglou, S. Schramm, J. Schaffner-Bielich, H. Stöcker, and W. Greiner, Phys. Rev. C **63**, 025211 (2001).
[122] H. Lenske and M. Dhar, Lect. Notes Phys. **948**, 161 (2018).
[123] N. K. Glendenning, Phys. Lett. **114B**, 392 (1982).
[124] J. C. T. Oliveira, H. Rodrigues, and S. B. Duarte, J. Phys. Conf. Ser. **1291**, 012038 (2019).
[125] A. R. Raduta, M. Oertel, and A. Sedrakian, Mon. Not. R. Astron. Soc. **499**, 914 (2020).
[126] V. Dexheimer, K. D. Marquez, and D. P. Menezes, Eur. Phys. J. A **57**, 216 (2021).
[127] P. Alba, V. M. Sarti, J. Noronha-Hostler, P. Parotto, I. Portillo-Vazquez, C. Ratti, and J. M. Stafford, Phys. Rev. C **101**, 054905 (2020).
[128] S. Weinberg, Phys. Rev. **166**, 1568 (1968).
[129] W. Bardeen and B. Lee, Phys. Rev. C **177**, 2389 (1969).
[130] A. Mishra, A. Kumar, S. Sanyal, and S. Schramm, Eur. Phys. J. A **41**, 205 (2009).
[131] A. Mishra, S. Schramm, and W. Greiner, Phys. Rev. C **78**, 024901 (2008).
[132] T. Barnes and E. S. Swanson, Phys. Rev. C **49**, 1166 (1994).
[133] C. M. Ko, P. Lévai, X. J. Qiu, and C. T. Li, Phys. Rev. C **45**, 1400 (1992).
[134] F. Klingl, N. Kaiser, and W. Weise, Z. Phys. A **356**, 193 (1996).
[135] G. Krein, A. W. Thomas, and K. Tsushima, Phys. Lett. B **697**, 136 (2011).

[136] K. L. Haglin and C. Gale, Nucl. Phys. **B421**, 613 (1994).
[137] C. Gale and J. I. Kapusta, Nucl. Phys. **B357**, 65 (1991).
[138] C. Song, Phys. Lett. B **388**, 141 (1996).
[139] F. E. Close and E. S. Swanson, Phys. Rev. D **72**, 094004 (2005).
[140] S. Godfrey and N. Isgur, Phys. Rev. D **32**, 189 (1985).
[141] G.-Q. Li and C. M. Ko, Nucl. Phys. **A582**, 731 (1995).
[142] P. Gubler and W. Weise, Nucl. Phys. **A954**, 125 (2016).
[143] D. Cabrera and M. J. Vicente Vacas, Phys. Rev. C **67**, 045203 (2003).
[144] J. Weil *et al.*, Proc. Sci. BORMIO2011 (**2011**) 053.
[145] H. W. Barz *et al.*, Open Nucl. Part. Phys. J. **3**, 1 (2010).
[146] K. Aoki *et al.*, Few Body Syst. **64**, 63 (2023).
[147] M. Destefanis, Nucl. Phys. **B245**, 199 (2013).